Journal of Physical and Chemical Reference Data

Recommended Cross Sections for Electron–Indium Scattering

Cite as: J. Phys. Chem. Ref. Data **50**, 013101 (2021); https://doi.org/10.1063/5.0035218
Submitted: 27 October 2020 . Accepted: 03 December 2020 . Published Online: 29 January 2021

K. R. Hamilton, O. Zatsarinny, K. Bartschat, M. S. Rabasović, D. Šević, B. P. Marinković, S. Dujko, J. Atić, D. V. Fursa, I. Bray, R. P. McEachran, F. Blanco, G. García, P. W. Stokes, R. D. White, D. B. Jones, L. Campbell, and M. J. Brunger

Journal of Physical and Chemical Reference Data ARTICLE scitation.org/journal/jpr

Recommended Cross Sections for Electron–Indium Scattering

Cite as: J. Phys. Chem. Ref. Data 50, 013101 (2021); doi: 10.1063/5.0035218
Submitted: 27 October 2020 • Accepted: 3 December 2020 •
Published Online: 29 January 2021

View Online Export Citation CrossMark

K. R. Hamilton,[1] O. Zatsarinny,[1] K. Bartschat,[1] M. S. Rabasović,[2] D. Šević,[2] B. P. Marinković,[2] S. Dujko,[2] J. Atić,[2] D. V. Fursa,[3] I. Bray,[3] R. P. McEachran,[4] F. Blanco,[5] G. García,[6] P. W. Stokes,[7] R. D. White,[7] D. B. Jones,[8] L. Campbell,[8] and M. J. Brunger[8,9,a)]

AFFILIATIONS

[1]Department of Physics and Astronomy, Drake University, Des Moines, Iowa 50311, USA
[2]Institute of Physics Belgrade, University of Belgrade, Pregrevica 118, 11080 Belgrade, Serbia
[3]Curtin Insititute for Computation and Department of Physics and Astronomy, Perth 6102, WA, Austraila
[4]Laser Physics Centre, RSP, Australian National University, Canberra, ACT 0200, Australia
[5]Departamento de Estructura de La Materia, Física Térmica y Electrónica e IPARCOS, Universidad Complutense de Madrid, Avenida Complutense, E-28040 Madrid, Spain
[6]Instituto de Física Fundamental, CSIC, Serrano 113-bis, E-28006 Madrid, Spain
[7]College of Science and Engineering, James Cook University, Townsville, Queensland 4810, Australia
[8]College of Science and Engineering, Flinders University, GPO Box 2100, Adelaide, SA 5001, Australia
[9]Department of Actuarial Science and Applied Statistics, Faculty of Business and Management, UCSI University, Kuala Lumpur 56000, Malaysia

[a)]**Author to whom correspondence should be addressed:** michael.brunger@flinders.edu.au

ABSTRACT

We report, over an extended energy range, recommended angle-integrated cross sections for elastic scattering, discrete inelastic scattering processes, and the total ionization cross section for electron scattering from atomic indium. In addition, from those angle-integrated cross sections, a grand total cross section is subsequently derived. To construct those recommended cross-section databases, results from original B-spline R-matrix, relativistic convergent close-coupling, and relativistic optical-potential computations are also presented here. Electron transport coefficients are subsequently calculated, using our recommended database, for reduced electric fields ranging from 0.01 Td to 10 000 Td using a multiterm solution of Boltzmann's equation. To facilitate those simulations, a recommended elastic momentum transfer cross-section set is also constructed and presented here.

Published by AIP Publishing on behalf of the National Institute of Standards and Technology. https://doi.org/10.1063/5.0035218

Key words: electron scattering cross sections; electron transport; recommended cross-section data; indium.

CONTENTS

List of Tables

List of Figures

1. Introduction

In our recent experimental and theoretical study on the electron-impact excitation of the $(5s^25p)^2P_{1/2} \rightarrow (5s^26s)^2S_{1/2}$ transition in indium (In),[1] we outlined a number of basic-science and applied rationales for why indium is a target of general interest. Of particular relevance to this work, where we attempt to compile a complete cross-section database over a wide energy range, is the need to have such a complete database in order to conduct quantitative modeling investigations for electron transport in indium under an applied electric field (e.g., Refs. 2 and 3) and for the collisional-radiative modeling of low-temperature plasmas where indium is one of the constituent species.[4] Note that the importance of having such a comprehensive database available for these types of simulations is discussed in detail in Ref. 5 and indeed is one of the prime drivers behind the establishment of the LXCat project.[6] Another important technological application of indium is its role as a tracer in two-line atomic fluorescence thermometry measurements.[7] This approach employs two diode lasers with wavelengths of 410 nm and 451 nm, in order to excite the $(5s^26s)^2S_{1/2}$ resonance state of indium atoms seeded into a flame. Owing to the typically greater oscillator strengths of atoms compared to molecules, strong fluorescence signals can be obtained at lower excitation energies. A particular plus of indium atoms is that its spin–orbit coupling in the $5p$ ground state leads to an energy spacing of ≈kT in standard combustion environments (2000 K–4000 K).[8]

The only previous elastic angle-integrated cross-section (ICS) results available in the literature are due to Rabasović *et al.*[9] In that study, experimental ICSs were determined, from extrapolation and integration of their elastic differential cross sections, for incident electron energies (E_0) between 10 eV and 100 eV. Corresponding atomic optical-potential (OP) calculations, but now for $E_0 = 10$ eV to 350 eV, were also reported.[9] As this previous study does not cover a comprehensive enough energy range for swarm or plasma simulation investigations and as further independent assessments of their results would be desirable, here, we report additional OP results and the results from a static-exchange plus polarization (SEP) theoretical approach, as well as the corresponding elastic cross sections from our relativistic B-spline R-matrix (DBSR) and relativistic convergent close-coupling (RCCC-75) computations from the work of Hamilton *et al.*[1] With these new theoretical results, we are confident that a recommended elastic ICS database, for $E_0 = 0.001$ eV–10 000 eV, can now be constructed.

The situation is even worse for the case of excitation of the discrete inelastic states in indium. Aside from a set of nine angle-ICSs contained in the paper of Ögün *et al.*,[4] five of which were for excitation from the $(5s^25p)^2P_{1/2}$ ground state and a further four of which were for excitation from the close-lying $(5s^25p)^2P_{3/2}$ metastable state, as well as our results for the single $(5s^25p)^2P_{1/2} \rightarrow (5s^26s)^2S_{1/2}$ excitation process discussed in Ref. 1, we know of no other available results in the literature. The ICSs reported in Ref. 4 were calculated using the method of Gryziński,[10,11] which is not *ab initio* in its construction so that their data are unlikely to be accurate. As a consequence, we do not consider those results further here. On the other hand, we found excellent agreement between our DBSR, RCCC, and measured cross-section results for the $(5s^25p)^2P_{1/2} \rightarrow (5s^26s)^2S_{1/2}$ transition.[1] This gives us hope that these DBSR and RCCC computations can provide us with accurate and reliable data for a total of 42 discrete inelastic excitation processes as well as the summed ICS for these discrete excitations (which can be compared with corresponding results from our atomic OP calculations), from which an extensive recommended cross-section database can be constructed.

With regard to the total ionization cross section (TICS), however, there has been a quite significant body of earlier work already undertaken. This includes experimental results from the work of Vainshtein *et al.*,[12] Shimon *et al.*,[13] and Shul *et al.*,[14] as well as various types of calculations such as a semi-empirical result from the work of Lotz,[15] an empirical TICS from the work of Talukder *et al.*,[16] a Deutsch–Märk method result from the work of Margreiter *et al.*,[17] and a binary encounter Bethe (BEB) formulation TICS from the work of Kim and Stone.[18] Note that in that latter study, plane-wave-Born (PWB) calculations for some of the more important autoionizing states were also undertaken, in order to present a more physical determination of the TICS. Furthermore, note that the measurement

of Shimon *et al.*[13] displays an unphysical shape, possessing a local minimum in the TICS at an energy where one might expect to find a maximum cross section. As a consequence, the results from the work of Shimon *et al.*[13] do not figure in our further deliberations. Unfortunately, despite all this earlier work into indium's TICS, as we shall shortly see, the level of accord between those various measurements and calculations[12–18] is only marginal. Hence, in this paper, we also present TICS results from our RCCC-75, DBSR-214, and atomic OP calculations, as well as our own BEB calculation with a superior model chemistry over that used in Ref. 18 to try and clarify matters prior to constructing a recommended TICS.

The remainder of this paper is constructed as follows. In Sec. 2, we detail our theoretical approaches that were used to compute new cross sections for this investigation. Thereafter, in Sec. 3, a detailed comparison of all the available elastic ICS, discrete inelastic ICS, and TICS is provided with our recommended cross sections, which result from each of these comparisons, also being formed here. In Sec. 4, we apply our recommended electron–indium database, to study the behavior of an electron swarm, under the influence of an applied external electric field, with various transport coefficients[2,3] being derived. Finally, in Sec. 5, some conclusions from this investigation will be drawn.

2. Theory Details

In Ref. 1, an appropriate description of both our RCCC-75 and DBSR-214 calculations was given, to which we refer the interested reader. Note, however, that here we have extended our original RCCC-75 computations[1] to 7000 eV for both the elastic ICS and momentum transfer cross sections (MTCSs) and to 10 000 eV for the sum over all inelastic ICSs. In addition, as a part of this study, we reran our RCCC-75 calculations with a somewhat more sophisticated target description (dipole polarizability = 53.128 a_0^3 vs 40.3 a_0^3 in Ref. 1) than that employed in Ref. 1. However, at higher energies, the RCCC-75 elastic ICS and MTCS are basically identical irrespective of which target description is employed. Similarly, even though the summed discrete inelastic ICS is a little higher in magnitude, as a function of energy, with the new target description compared to that of Hamilton *et al.*,[1] both sets of results have the same energy dependence at higher energies. As one of the main aims of this study is to determine a recommended database for e^- + In scattering, the above observations suggest that, in terms of possibly using the RCCC-75 results to effect a higher-energy extrapolation (see later), cross sections from either target description are equally valid. Under those circumstances, we have continued to employ the RCCC-75 results from the work of Hamilton *et al.*[1] throughout this paper. Additional calculations using our atomic-optical approach, a SEP method, and our own application of the BEB procedure[5] are presented here, so a brief description of each of them is now given below.

2.1. OP model

We have recently described our standard OP approach in our studies of the electron–beryllium,[19] electron–magnesium,[20] electron–zinc,[21] and electron–bismuth[22] scattering systems. The generic details of this atomic OP method were given in those papers so that only the key points of this approach are summarized below.

The projectile–atom interaction is described by a local complex potential given by

$$V(r) = V_s(r) + V_{ex}(r) + V_{pol}(r) + iV_{abs}(r), \quad (1)$$

where the real part of the potential is comprised of the following three terms. V_s is the static term derived from a Hartree–Fock calculation[23] of the atomic charge distribution. V_{ex} is an exchange term that accounts for the indistinguishability of the incident and target electrons; it is given by the semi-classical energy dependent formula derived by Riley and Truhlar.[24] Finally, V_{pol} is a polarization potential for the long–range interactions that depend on the target dipole polarizability. For this study, the polarization potential of Ref. 25, leading to results we denote as OP1, and that of Ref. 26, leading to cross sections we denote as OP2, were both applied.

The imaginary absorption potential accounts for the inelastic, both discrete and continuum, scattering events. It is based on the quasi-free model put forward by Staszewska *et al.*[27] but incorporates some improvements to the original formulation. These include allowing for the inclusion of screening effects, local velocity corrections, and the description of the electron indistinguishability,[28] leading to a model that provides a realistic approximation for electron–atom scattering over a broad energy range.[29]

The present atomic optical model is non-relativistic in formulation and leads to angle-integrated elastic cross sections, the sum over all discrete inelastic angle-ICSs, and the TICS. Note that as indium is only a moderately heavy atom, the differences in the calculated scattering cross sections between a relativistic and non-relativistic treatment will not be significant. As a consequence, the application of our non-relativistic OP approach is valid for this target.

2.2. SEP method

Our SEP model includes both relativistic static and polarization potentials as well as the exchange interaction. The spin–orbit interaction in indium gives rise to two "ground-state" levels, namely, $(5s^25p)^2P_{1/2}$ and $(5s^25p)^2P_{3/2}$ with the $j = 3/2$ state being ~0.274 eV above the $j = 1/2$ state. A linear combination of the wavefunctions corresponding to these two states was then employed in a 2-state Dirac–Fock multiconfiguration calculation[30,31] to determine the ground-state configuration of In within a frozen-core model. The static potential was then determined in the usual manner.

The dipole polarization was determined using the relativistic non-perturbative polarized-orbital method for alkali and alkali-like atoms.[26] Finally, the exchange interaction was accounted for by antisymmetrization of the total scattering wavefunction. This approach only yields elastic scattering cross sections, and since it does not include any inelastic processes, it is expected to become less reliable as the energy of the incident electron increases.

2.3. BEB approach

Kim and Stone[18] calculated the TICS for indium using the BEB formalism.[5,32] The BEB approach is sensitive to the binding energies used in the calculation, so we have repeated the work of Kim and Stone[18] using an improved structural representation for indium based on the best available experimental data for the orbital binding energies. Those values have been assembled from the available photoionization spectra[33,34] and information regarding the convergence of spectral lines to the ionization thresholds.[35,36] These values have been combined with orbital kinetic energies for atomic indium that were derived from a single point energy calculation of indium hydride

TABLE 1. Parameters used for the present BEB TICS calculation of atomic indium. See also supplementary material, Table S1

Orbital	B_i (eV)	U_i (eV)	N_i	η_{pqn}
$5p$	5.79	27.94	1	5
$5s$	11.16	53.70	2	5
$4d_{5/2}$	24.4	282.35	6	4
$4d_{3/2}$	25.7	282.35	4	4
$4p_{3/2}$	86.0	441.12	4	4
$4p_{1/2}$	95.4	441.12	2	4
$4s$	126.0	496.51	2	4
$3d_{5/2}$	468.5	1735.41	6	3
$3d_{3/2}$	476.4	1735.41	4	3
$3p_{3/2}$	691.8	1844.65	4	3
$3p_{1/2}$	731.3	1844.65	2	3
$3s$	854.4	1894.15	2	3

(InH, r = 9.0 Å) in Gaussian 09,[37] with the model chemistry employing density functional theory (B3LYP)[38] and a double zeta valance polarized basis set.[39] The parameters used in the present BEB calculation are summarized in Table 1.

Within the BEB formalism,[32] the TICS is obtained by summing up the contributions from each populated orbital, with the ith orbital's contribution being given by

$$Q_i(t_i) = \frac{4\pi a_0^2 N_i}{t_i + \frac{u_i+1}{\eta_{pqn}}}\left(\frac{R}{B_i}\right)^2\left[\frac{\ln t_i}{2}\left(1-\frac{1}{t_i^2}\right)+1-\frac{1}{t_i}-\frac{\ln t_i}{t_i+1}\right]. \quad (2)$$

In Eq. (2), the binding energy of the ionized orbital, B_i, is used to scale the incident electron-impact energy (E_0) and orbital kinetic energies (u_i): $t_i = \frac{E_0}{B_i}$ and $u_i = \frac{U_i}{B_i}$, respectively. N_i is the orbital occupation number, while R and a_0 are, respectively, the Rydberg constant and Bohr radius. A modification to the traditional BEB approach comes when dealing with heavier elements, where the scaled kinetic energy is corrected by the principal quantum number of the ionized atomic orbital (η_{pqn}) if it is greater than 2.

3. Cross Section Assessment and Recommended Data

3.1. Elastic scattering

In Fig. 1, we summarize the available experimental and theoretical elastic angle-ICSs for electron–indium scattering, including original results from computations associated with this study. It is quite clear from this figure that between 10 eV and 90 eV, the experimental data of Rabasović *et al.*[9] are, to within the cited error bars, in very good agreement with their optical-model SEPASo[9] computation and our OP1, SEP, and DBSR-214 calculations. Agreement with our RCCC-75 calculation is also typically fair over this energy range. This level of accord, between experiment and theory, in that energy regime is by no means unique to indium, having also been observed by us in our recent study of elastic electron scattering from bismuth.[22] Similarly, but now for energies in the range 1 eV–10 eV, we find good levels of accord between our OP1, RCCC-75, and DBSR-214 calculations. Below 1 eV, however, there is quite a significant level of discrepancy between all the available theoretical results. While all the theories predict a significant structure, which would arise due to the temporary capture of the incident electron by the target, in the elastic ICS, the position (in the range ~0.09 eV–0.2 eV) and magnitude (~200 $\times 10^{-16}$ cm^2–700 $\times 10^{-16}$ cm^2) of that peak are seen to vary from one theory to another. Our non-relativistic OP1, OP2, and SEP calculations all show this structure arising in the $\ell = 1$ (i.e., p-wave) partial wave, suggesting that the origin of this feature is consistent with a p-wave shape resonance. For our relativistic RCCC and DBSR computations, the structure is in the $J = 2$, parity = +1, partial wave of the total scattering system. As the $(5s^2 5p)^2 P_{1/2}$ ground state has $j = 1/2$, parity = −1, this leads to the projectile waves of either $j = 3/2$, parity = −1, $\ell = 1$ or j = 5/2, parity = −1, $\ell = 3$. Normally, we would expect it, consistent with our non-relativistic results, to be in $\ell = 1$, as $\ell = 3$ is too large for the centrifugal barrier to support a resonance. It is interesting to note that it is known[40] that the $(5s^2 5p^2)^3 P_{0,1,2}$ and $(5s^2 5p^2)\ ^1D_2$ and $^1S_0$ states of the negative indium ion are stable, with, for example, the $^3P_0$ state having an electron affinity of 384 meV, the $^3P_1$ state having an electron affinity of 460 meV, and the $^3P_2$ state having an electron affinity of 555 meV. Under these circumstances, a low-energy electron could simply bind to the indium atom to form In^-, which may have consequences for electron swarm behavior[2,3] at low E/n_0 (E = applied external electric field and n_0 = background gas density number). To quantitatively specify whether the structure we observe in Fig. 1 is a resonance or simply an artifact of our computational methods, we would need to do a significantly more accurate structure calculation for both In and In^- and

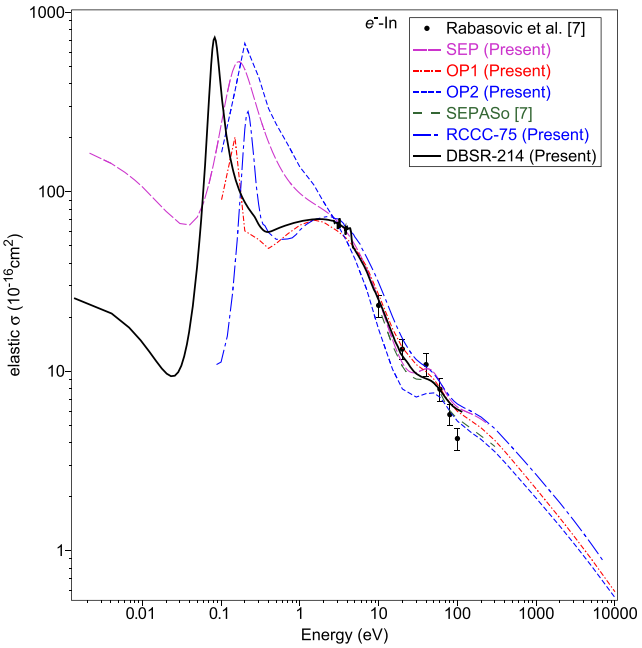

FIG. 1. Angle-integrated elastic cross sections ($\times 10^{-16}$ cm^2) for electron scattering from In. Results from the present relativistic SEP (purple dashed line); non-relativistic OP, (red dotted-dashed line) OP1 and (blue dashed line) OP2; and relativistic RCCC-75 (blue dotted-dashed line) and DBSR-214 (black solid line) computations, as well as the experimental (black circles) and SEPASo theory (green dashed line) results from the work of Rabasović *et al.*,[9] are plotted.

Published by AIP Publishing on behalf of the National Institute of Standards and Technology.

TABLE 2. Recommended elastic ICS, MTCS, summed discrete inelastic (electronic-state) ICS, TICS, and grand total (TCS) cross sections ($\times 10^{-16}$ cm^2) for electron scattering from indium. See also supplementary material, Table S2

E_0 (eV)	Elastic ICS ($\times 10^{-16}$ cm^2)	MTCS ($\times 10^{-16}$ cm^2)	Σ discrete inelastic ($\times 10^{-16}$ cm^2)	TICS ($\times 10^{-16}$ cm^2)	TCS ($\times 10^{-16}$ cm^2)
1.361×10^{-3}	25.6	25.4			25.6
4.080×10^{-3}	21.0	20.6			21.0
4.082×10^{-3}	21.0	20.6			21.0
6.800×10^{-3}	17.5	16.9			17.5
9.520×10^{-3}	14.9	14.2			14.9
0.012 25	12.9	12.2			12.9
0.017 69	10.4	9.69			10.4
0.023 13	9.40	8.69			9.40
0.028 57	9.89	9.07			9.89
0.034 01	12.1	11.1			12.1
0.039 46	16.8	15.6			16.8
0.044 90	25.5	23.9			25.5
0.050 34	41.1	39.2			41.1
0.055 78	69.5	67.3			69.5
0.061 23	123	120			123
0.063 95	165	162			165
0.069 39	300	298			300
0.080 27	703	703			703
0.085 72	696	697			696
0.096 60	432	432			432
0.104 8	304	302			304
0.110 2	251	249			251
0.121 1	188	183			188
0.142 9	131	124			131
0.164 6	106	98.4			106
0.210 9	84.2	74.0			84.2
0.273 5	71.3	59.7	0.00		71.3
0.276 2	70.7	59.1	2.25		72.9
0.278 9	70.0	58.2	3.46		73.5
0.287 1	68.2	55.8	5.61		73.9
0.319 7	63.3	49.6	10.7		74.0
0.401 4	59.8	44.0	18.5		78.3
0.496 6	61.9	43.9	20.0		81.9
0.761 9	66.3	44.2	16.7		83.0
1.075	68.9	44.3	13.5		82.4
1.673	70.6	42.7	10.1		80.6
2.626	69.0	36.2	7.53		76.6
2.721	69.0	35.8	7.04		76.0
2.762	67.0	34.1	7.82		74.8
3.018	65.8	33.0	7.23		73.1
3.020	64.1	33.0	7.73		71.8
3.023	62.1	32.9	9.48		71.5
3.034	66.6	32.3	7.64		74.2
3.184	68.0	32.1	6.77		74.8
3.186	71.3	31.8	6.97		78.3
3.189	63.0	31.5	8.97		72.0
3.192	64.5	31.2	7.66		72.1
3.211	65.6	30.8	7.20		72.8
3.765	60.8	25.8	7.99		68.8
3.769	62.0	25.6	7.62		69.6
3.791	61.2	25.2	8.22		69.4
3.804	58.3	23.9	10.1		68.3

Published by AIP Publishing on behalf of the National Institute of Standards and Technology.

TABLE 2. (*Continued.*)

E_0 (eV)	Elastic ICS ($\times 10^{-16}$ cm^2)	MTCS ($\times 10^{-16}$ cm^2)	Σ discrete inelastic ($\times 10^{-16}$ cm^2)	TICS ($\times 10^{-16}$ cm^2)	TCS ($\times 10^{-16}$ cm^2)
3.810	62.0	23.5	8.70		70.7
3.823	63.2	24.8	7.95		71.2
3.908	63.1	25.3	7.43		70.6
3.913	62.4	25.4	7.92		70.3
3.921	63.6	25.5	7.40		71.0
4.327	62.9	21.2	9.91		72.8
4.531	55.2	16.5	13.4		68.6
4.612	51.9	15.5	13.6		65.5
4.776	48.8	15.3	12.2		61.0
5.786	42.6	11.7	11.3	0.00	53.9
6.00	41.4	11.3	11.2	0.310	52.9
8.71	28.5	5.60	8.95	3.46	40.9
10.0	25.0	4.40	7.99	4.96	37.9
12.4	20.0	3.46	7.14	6.68	33.8
16.2	14.7	2.56	6.65	8.38	29.7
20.0	12.2	2.02	6.39	9.24	27.8
30.0	9.71	2.98	5.81	9.78	25.3
40.0	9.11	4.49	5.37	9.29	23.8
46.4	8.84	4.36	5.08	8.87	22.8
65.0	7.51	4.07	4.35	7.87	19.7
80.0	6.66	3.13	3.93	7.21	17.8
95.0	6.22	2.53	3.60	6.66	16.5
120	5.80	2.04	3.12	5.96	14.9
150	5.42	1.81	2.68	5.36	13.5
200	4.96	1.64	2.18	4.66	11.8
300	4.22	1.41	1.61	3.79	9.62
400	3.66	1.17	1.28	3.20	8.15
600	2.97	0.865	0.923	2.59	6.49
800	2.55	0.656	0.730	2.23	5.51
1 000	2.27	0.517	0.607	1.98	4.86
2 000	1.56	0.224	0.337	1.35	3.24
3 000	1.24	0.131	0.235	1.06	2.54
4 000	1.05	0.0877	0.179	0.887	2.12
5 000	0.924	0.0637	0.144	0.771	1.84
6 000	0.826	0.0489	0.120	0.682	1.63
8 000	0.693	0.0315	0.0888	0.561	1.34
10 000	0.605	0.0221	0.0701	0.482	1.16

to perform our scattering calculations on a much finer energy grid. This is beyond the scope of this publication. Nonetheless, in spite of the above caveats, it is crucial in modeling/simulation applications to have a complete cross-section database.[5] As a consequence, given it is our most detailed relativistic *ab initio* computation, and in what follows, for energies below 1 eV, we recommend our DBSR-214 elastic ICS results. Note that at low energies, the dipole polarizability plays a very important role in the elastic scattering dynamics.[41,42] In our current work, the static dipole polarizability (α_d) of the In atom in the RCCC-75 model is 40.3 a_0^3 and in our DBSR-214 model is 61.3 a_0^3, while the experimental value is ~68.69 a_0^3.[43] We believe that these differences between theory and experiment in α_d explain, at least in part, the different peak positions and magnitudes in the elastic ICS low-energy structures and further indicate that even more detailed structure descriptions are warranted at some stage.

On the basis of the above discussion and the results shown in Fig. 1, we form our recommended elastic ICS from our DBSR-214 result from 0.001 eV to 100 eV and from a suitably scaled, to maintain continuity (scaling factor = 1.025), OP1 result from 100 eV to 10 000 eV. This recommended elastic ICS is listed in Table 2 for a selection of incident electron energies, and we estimate the uncertainty on it to be ~±20% for energies less than 3 eV and ~±15% for energies greater than 3 eV. Note that the sensitivity of our recommended cross sections to our choice of normalization energy was investigated both here and for all the later scattering processes we consider. We found that our recommended cross sections, for $E_0 \geqslant 100$ eV, were largely insensitive to our choice of normalization energy between 70 eV and 100 eV. This result gives us confidence in the robustness of our higher energy recommended cross sections. The elastic MTCS is also very important for electron transport simulations, with much of the discussion just given for the elastic ICS also

Published by AIP Publishing on behalf of the National Institute of Standards and Technology.

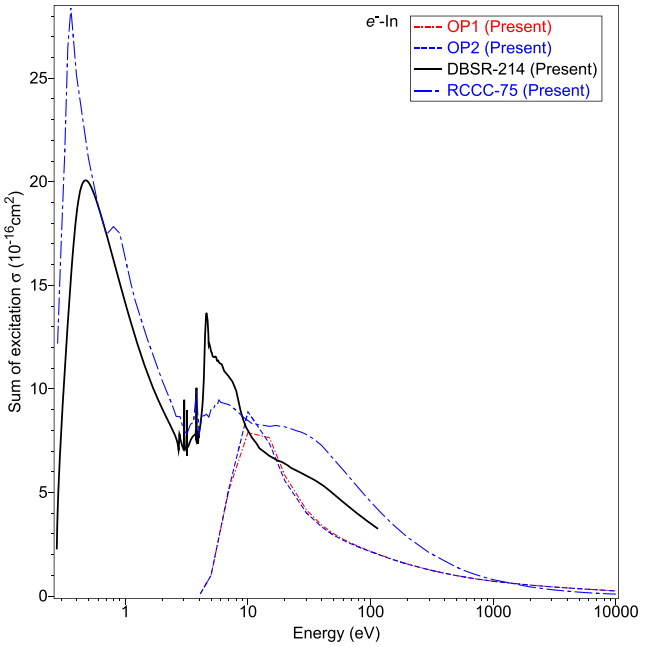

FIG. 2. Summed discrete inelastic cross sections ($\times 10^{-16}$ cm^2) for electron-impact excitation of In. Present non-relativistic OP, (red dotted-dashed line) OP1 and (blue dashed line) OP2, and relativistic RCCC-75 (blue dotted-dashed line) and DBSR-214 (black line) computational results are plotted.

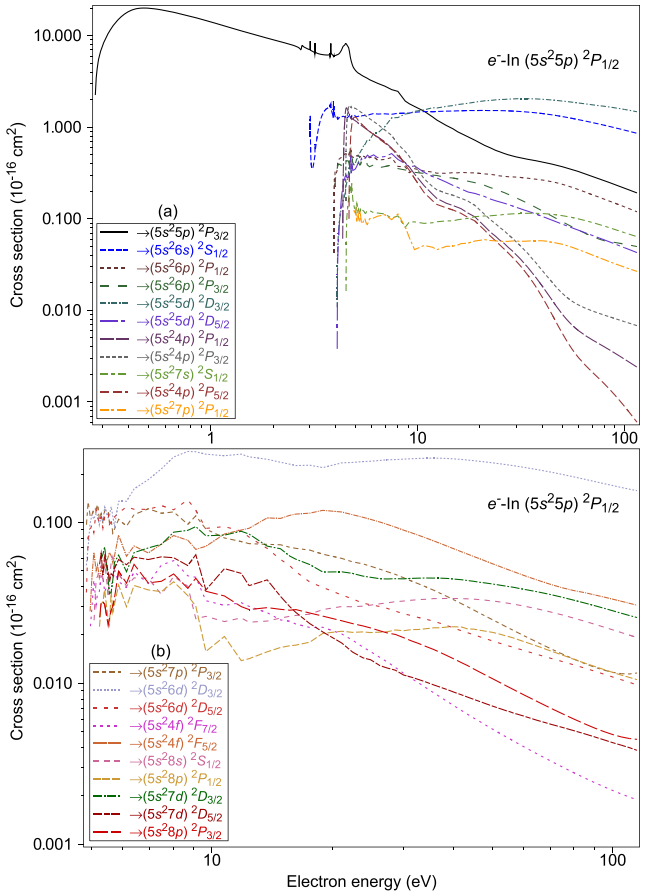

FIG. 3. Individual discrete inelastic cross sections ($\times 10^{-16}$ cm^2) for electron-impact excitation of In from the $(5s^2 5p)\ ^2P_{1/2}$ ground state to the higher-lying excited states as denoted in legends (a) and (b). All results are from our DBSR-214 calculation, and they represent our recommended data for each of these processes.

being applicable to it. As a consequence, we do not repeat that detail; rather, we simply note that our recommended MTCS is formed from our DBSR-214 calculation for 0.001 eV–100 eV and from our RCCC-75 result, again suitably scaled to ensure continuity (scaling factor = 0.9564) for 100 eV–7000 eV. Finally, for 7 keV–10 keV, we use our scaled OP1 result (scaling factor = 2.653) to complete our MTCS database. That recommended MTCS can also be found in Table 2, with an uncertainty on it of ~±20% for energies less than 3 eV and ~±15% for energies greater than 3 eV.

3.2. Discrete inelastic cross sections

We next consider the sum of all the discrete inelastic excited-state angle-ICSs, where only data from our OP1, OP2, RCCC-75, and DBSR-214 calculations are available. Those results are plotted in Fig. 2, where several observations are immediately apparent. First, while our OP1 and OP2 results agree well with one another, both appear to predict an incorrect threshold for the opening of inelastic excitation, and as a consequence, both predict a maximum in the summed cross section to occur at too high an incident electron energy. This is not unexpected as the OP1 and OP2 models do not account for the fine-structure splitting of the ground state. So their lowest inelastic threshold is at around 3 eV for the $(5s^2 6s)^2S_{1/2}$ state, while the actual value is ~0.27 eV for the $(5s^2 5p)^2P_{3/2}$ state. In addition, both the OP1 and OP2 results are generally in poor accord with our relativistic RCCC-75 and DBSR-214 results. In our recent work[1] on the electron-impact excitation of the $(5s^2 5p)^2P_{1/2} \rightarrow (5s^2 6s)^2S_{1/2}$ transition, we found excellent agreement between our RCCC-75, DBSR-214, and measured angle-ICSs over their common energy range (to typically ~±10%). This level of accord between them is clearly not maintained in Fig. 2, a point that is in need of further interrogation, although we note that qualitatively the RCCC-75 and DBSR-214 results remain in fair agreement. The relatively marginal quantitative accord between our RCCC-75 and DBSR-214 computations, for the summed discrete angle-integrated inelastic cross sections in Fig. 2, we believe is due to an inaccuracy of the quasi one-electron RCCC model for In, at least for some inelastic transitions that are important. One example of that is for the $(5s^2 5p)^2P_{1/2} \rightarrow (5s^2 5d)^2D_{3/2}$ transition, where the optical oscillator strength in the RCCC target-state description has a value of 0.451, which is substantially higher than those from our DBSR calculations (0.341)[1] and the corresponding NIST value (0.36).[35] The effect of this carries through in the respective RCCC-75 and DBSR-214 scattering results, where the magnitude of the RCCC $(5s^2 5d)^2D_{3/2}$ ICS would be anticipated to be greater than that for the DBSR-214 $(5s^2 5d)^2D_{3/2}$ ICS. This observation is entirely consistent, away from the influence of resonance-effects, with what we found in Fig. 2. As a consequence, for the summed discrete inelastic ICS, our recommended database is here formed from the DBSR-214 results from

Published by AIP Publishing on behalf of the National Institute of Standards and Technology.

TABLE 3. Angle-ICSs (10^{-16} cm^2) at 90 incident electron energies, selected to show any structure for electron–indium scattering from the $(5s^2 5p)\ ^2P_{1/2}$ ground state. See also supplementary material, Table S3a

	Cross section (10^{-16} cm^2)											
	$\rightarrow (5s^2 5p)\ ^2P_{3/2}$		$\rightarrow (5s^2 6p)\ ^2P_{1/2}$		$\rightarrow (5s^2 5d)\ ^2D_{3/2}$		$\rightarrow (5s^2 4p)\ ^2P_{1/2}$		$\rightarrow (5s^2 7s)\ ^2S_{1/2}$		$\rightarrow (5s^2 7p)\ ^2P_{1/2}$	
Energy (eV)		$\rightarrow (5s^2 6s)\ ^2S_{1/2}$		$\rightarrow (5s^2 6p)\ ^2P_{3/2}$		$\rightarrow (5s^2 5d)\ ^2D_{5/2}$		$\rightarrow (5s^2 4p)\ ^2P_{3/2}$		$\rightarrow (5s^2 4p)\ ^2P_{5/2}$		
0.2743	0.00											
0.2762	2.25											
0.2789	3.46											
0.3088	9.26											
0.3524	14.5											
0.3796	17.1											
0.4476	19.9											
0.5102	19.9											
0.5714	19.2											
0.6803	17.8											
0.8027	16.2											
0.8708	15.4											
0.9796	14.3											
1.116	13.2											
1.265	12.1											
1.483	10.9											
1.673	10.1											
1.823	9.57											
2.041	8.93											
2.259	8.40											
2.653	7.44											
3.022	8.25	0.00										
3.025	8.01	1.37										
3.033	7.01	0.716										
3.041	6.93	0.506										
3.061	6.86	0.381										
3.116	6.72	0.364										
3.186	6.47	0.497										
3.189	8.32	0.657										
3.770	5.82	1.74										
3.804	8.25	1.80										
3.815	6.59	1.60										
3.908	6.07	1.37										
3.913	6.01	1.91										
3.921	5.88	1.52										
3.945	5.96	1.70	0.00									
3.946	5.93	1.71	0.0389									
3.951	6.03	1.43	0.249									
3.973	6.06	1.36	0.226									
3.982	6.07	1.33	0.296	0.00								
3.986	6.08	1.31	0.332	0.182								
4.014	6.10	1.27	0.314	0.293								
4.078	6.20	1.30	0.340	0.353	0.00							
4.081	6.21	1.30	0.342	0.356	0.00832	0.00						

TABLE 3. (*Continued.*)

Energy (eV)	Cross section (10^{-16} cm^2)										
	$\rightarrow (5s^2 5p)\ ^2P_{3/2}$		$\rightarrow (5s^2 6p)\ ^2P_{1/2}$		$\rightarrow (5s^2 5d)\ ^2D_{3/2}$		$\rightarrow (5s^2 4p)\ ^2P_{1/2}$		$\rightarrow (5s^2 7s)\ ^2S_{1/2}$		$\rightarrow (5s^2 7p)\ ^2P_{1/2}$
	$\rightarrow (5s^2 6s)\ ^2S_{1/2}$		$\rightarrow (5s^2 6p)\ ^2P_{3/2}$		$\rightarrow (5s^2 5d)\ ^2D_{5/2}$		$\rightarrow (5s^2 4p)\ ^2P_{3/2}$		$\rightarrow (5s^2 4p)\ ^2P_{5/2}$		
4.082	6.21	1.30	0.343	0.356	0.0103	0.00348					
4.095	6.21	1.24	0.385	0.365	0.0360	0.0242					
4.150	6.31	1.25	0.444	0.396	0.0769	0.0713					
4.337	7.47	1.31	0.476	0.407	0.151	0.213	0.00				
4.340	7.50	1.31	0.477	0.408	0.153	0.215	0.0570				
4.466	8.13	1.30	0.515	0.454	0.196	0.291	1.42	0.00			
4.501	8.22	1.25	0.514	0.437	0.225	0.303	1.60	0.506	0.00		
4.503	8.22	1.24	0.514	0.433	0.227	0.303	1.61	0.546	0.0149		
4.531	8.06	1.25	0.512	0.425	0.243	0.288	1.63	0.937	0.0855		
4.643	7.31	1.32	0.516	0.422	0.339	0.290	1.42	1.71	0.172	0.00	
4.667	6.91	1.34	0.515	0.402	0.388	0.282	1.37	1.74	0.190	0.216	
4.748	5.53	1.31	0.564	0.555	0.403	0.496	1.27	1.66	0.205	0.841	
4.776	5.27	1.27	0.550	0.442	0.311	0.320	1.24	1.64	0.191	0.971	
4.818	4.92	1.33	0.475	0.421	0.401	0.359	1.24	1.64	0.217	1.11	0.00
4.830	4.83	1.33	0.474	0.444	0.402	0.376	1.24	1.64	0.197	1.14	0.130
5.020	4.15	1.31	0.467	0.387	0.417	0.357	1.17	1.60	0.116	1.29	0.130
5.075	4.04	1.31	0.490	0.421	0.451	0.376	1.15	1.58	0.148	1.26	0.0941
5.143	3.94	1.32	0.484	0.390	0.457	0.402	1.12	1.54	0.123	1.20	0.124
5.238	3.84	1.35	0.468	0.389	0.522	0.427	1.08	1.50	0.111	1.14	0.0920
5.293	3.77	1.33	0.478	0.391	0.540	0.427	1.06	1.47	0.127	1.12	0.111
5.347	3.72	1.33	0.500	0.427	0.568	0.457	1.04	1.45	0.120	1.09	0.0913
5.850	3.31	1.38	0.465	0.371	0.720	0.475	0.901	1.24	0.123	0.901	0.100
6.94	2.82	1.40	0.445	0.373	1.02	0.479	0.692	0.936	0.113	0.674	0.111
8.03	2.47	1.42	0.374	0.354	1.28	0.446	0.485	0.654	0.108	0.516	0.113
8.71	1.93	1.43	0.370	0.342	1.40	0.400	0.411	0.545	0.0809	0.388	0.0819
9.66	1.69	1.46	0.353	0.322	1.49	0.379	0.309	0.382	0.0927	0.276	0.0461
10.7	1.50	1.49	0.333	0.313	1.55	0.322	0.230	0.274	0.0893	0.194	0.0513
12.4	1.20	1.49	0.315	0.298	1.62	0.280	0.167	0.208	0.0929	0.144	0.0460
14.8	0.962	1.51	0.320	0.279	1.73	0.232	0.140	0.181	0.0951	0.125	0.0504
17.6	0.785	1.53	0.319	0.258	1.83	0.196	0.115	0.156	0.101	0.103	0.0545
18.9	0.722	1.52	0.318	0.248	1.88	0.190	0.105	0.140	0.106	0.0949	0.0573
22.4	0.597	1.52	0.307	0.220	1.97	0.165	0.0718	0.0983	0.108	0.0650	0.0580
24.9	0.541	1.52	0.295	0.202	2.01	0.153	0.0588	0.0808	0.110	0.0522	0.0569
27.3	0.502	1.51	0.289	0.186	2.03	0.144	0.0491	0.0677	0.112	0.0427	0.0568
30.1	0.475	1.50	0.286	0.169	2.05	0.133	0.0402	0.0557	0.114	0.0342	0.0572
35.8	0.440	1.45	0.274	0.140	2.05	0.117	0.0258	0.0368	0.115	0.0209	0.0576
40.4	0.416	1.41	0.265	0.121	2.02	0.106	0.0179	0.0266	0.114	0.0135	0.0575
46.4	0.388	1.35	0.250	0.102	1.97	0.0936	0.0115	0.0184	0.111	0.00769	0.0547
50.2	0.370	1.31	0.238	0.0928	1.93	0.0874	0.00904	0.0153	0.108	0.00557	0.0527
57.8	0.337	1.23	0.215	0.0786	1.86	0.0775	0.00643	0.0120	0.102	0.00339	0.0476
65.0	0.309	1.17	0.195	0.0691	1.80	0.0702	0.00529	0.0105	0.0955	0.00250	0.0431
70.0	0.292	1.13	0.183	0.0642	1.76	0.0659	0.00477	0.00987	0.0912	0.00211	0.0403
80.0	0.261	1.05	0.164	0.0576	1.70	0.0589	0.00400	0.00889	0.0834	0.00158	0.0358
90.0	0.236	0.989	0.148	0.0552	1.63	0.0532	0.00341	0.00815	0.0765	0.00119	0.0324
105	0.208	0.907	0.130	0.0519	1.54	0.0464	0.00274	0.00728	0.0682	7.83×10^{-4}	0.0286
115	0.192	0.860	0.119	0.0499	1.48	0.0428	0.00240	0.00682	0.0640	6.02×10^{-4}	0.0267

Journal of Physical and Chemical Reference Data
ARTICLE
scitation.org/journal/jpr

TABLE 4. Angle-ICSs (10^{-16} cm^2) for electron–indium scattering from the $(5s^25p)\ ^2P_{1/2}$ ground state. See also supplementary material, Table S3b

	Cross section (10^{-16} cm^2)									
Energy (eV)	$\rightarrow (5s^27p)\ ^2P_{3/2}$	$\rightarrow (5p^26d)\ ^2D_{3/2}$	$\rightarrow (5s^26d)\ ^2D_{5/2}$	$\rightarrow (5s^24f)\ ^2F_{7/2}$	$\rightarrow (5s^24f)\ ^2F_{5/2}$	$\rightarrow (5p^28s)\ ^2S_{1/2}$	$\rightarrow (5s^28p)\ ^2P_{1/2}$	$\rightarrow (5s^27d)\ ^2D_{3/2}$	$\rightarrow (5P^27d)\ ^2D_{5/2}$	$\rightarrow (5s^28p)\ ^2P_{3/2}$
4.832	0.00									
4.841	0.0343	0.00								
4.848	0.0569	0.0207	0.00							
4.857	0.0921	0.0528	0.0332							
4.912	0.135	0.0709	0.0812							
4.923	0.130	0.0767	0.0831	0.00	0.00					
4.966	0.111	0.0984	0.0899	0.0212	0.0276					
5.020	0.110	0.112	0.0967	0.0298	0.0461					
5.038	0.114	0.109	0.0934	0.0345	0.0524	0.00				
5.075	0.122	0.105	0.0867	0.0440	0.0653	0.0229				
5.143	0.121	0.115	0.120	0.0308	0.0503	0.0448				
5.184	0.130	0.110	0.109	0.0364	0.0545	0.0462				
5.186	0.129	0.109	0.109	0.0365	0.0542	0.0464	0.00			
5.187	0.128	0.109	0.108	0.0365	0.0540	0.0465	4.81×10^{-4}	0.00		
5.190	0.127	0.108	0.108	0.0365	0.0534	0.0468	0.00180	0.00372	0.00	
5.193	0.126	0.108	0.107	0.0366	0.0530	0.0470	0.00281	0.00656	0.00271	0.00
5.238	0.105	0.0968	0.0987	0.0373	0.0453	0.0511	0.0218	0.0600	0.0537	0.0244
5.293	0.114	0.110	0.108	0.0467	0.0508	0.0538	0.0313	0.0592	0.0644	0.0321
5.347	0.0984	0.103	0.0924	0.0463	0.0494	0.0448	0.0321	0.0635	0.0472	0.0321
5.401	0.120	0.125	0.110	0.0369	0.0528	0.0585	0.0381	0.0704	0.0633	0.0310
5.510	0.119	0.107	0.116	0.0425	0.0612	0.0354	0.0246	0.0442	0.0491	0.0229
5.551	0.0994	0.111	0.0974	0.0458	0.0651	0.0451	0.0231	0.0361	0.0427	0.0254
5.606	0.104	0.126	0.101	0.0416	0.0622	0.0559	0.0373	0.0369	0.0481	0.0285
5.660	0.0857	0.110	0.0990	0.0424	0.0560	0.0612	0.0277	0.0439	0.0468	0.0301
5.714	0.0910	0.0951	0.108	0.0507	0.0620	0.0506	0.0310	0.0566	0.0520	0.0340
5.850	0.105	0.136	0.115	0.0430	0.0836	0.0481	0.0409	0.0627	0.0589	0.0499
6.12	0.0950	0.136	0.125	0.0394	0.0617	0.0403	0.0299	0.0494	0.0547	0.0420
6.39	0.112	0.162	0.121	0.0494	0.0715	0.0453	0.0406	0.0650	0.0609	0.0550
6.94	0.122	0.185	0.121	0.0418	0.0647	0.0450	0.0381	0.0696	0.0589	0.0421
7.48	0.114	0.216	0.127	0.0545	0.0735	0.0357	0.0372	0.0732	0.0612	0.0431
8.03	0.116	0.255	0.120	0.0580	0.0830	0.0462	0.0429	0.0871	0.0604	0.0479
8.71	0.0975	0.276	0.138	0.0466	0.0776	0.0402	0.0351	0.0894	0.0540	0.0390
9.12	0.110	0.275	0.119	0.0457	0.0681	0.0253	0.0302	0.0943	0.0631	0.0451
9.66	0.0911	0.266	0.0920	0.0327	0.0712	0.0261	0.0158	0.0828	0.0381	0.0374
10.7	0.0802	0.260	0.0943	0.0306	0.0849	0.0242	0.0196	0.0835	0.0517	0.0350
11.8	0.0761	0.266	0.0885	0.0318	0.0898	0.0255	0.0139	0.0882	0.0483	0.0300
12.4	0.0739	0.256	0.0812	0.0301	0.0921	0.0240	0.0143	0.0848	0.0405	0.0288
13.7	0.0732	0.247	0.0690	0.0275	0.107	0.0244	0.0157	0.0713	0.0440	0.0296
14.8	0.0727	0.237	0.0590	0.0248	0.106	0.0255	0.0167	0.0687	0.0348	0.0289
15.6	0.0702	0.230	0.0539	0.0243	0.111	0.0261	0.0171	0.0619	0.0300	0.0285
16.2	0.0691	0.226	0.0496	0.0234	0.113	0.0265	0.0173	0.0592	0.0276	0.0288
17.6	0.0674	0.227	0.0427	0.0223	0.114	0.0269	0.0181	0.0548	0.0235	0.0274
18.9	0.0636	0.219	0.0395	0.0223	0.119	0.0288	0.0205	0.0492	0.0209	0.0262
21.1	0.0598	0.235	0.0354	0.0203	0.116	0.0301	0.0211	0.0494	0.0178	0.0245
22.4	0.0570	0.236	0.0335	0.0186	0.112	0.0300	0.0208	0.0483	0.0157	0.0235

TABLE 4. (*Continued.*)

Energy (eV)	Cross section (10^{-16} cm^2)									
	$\rightarrow (5s^2 7p)\ ^2P_{3/2}$	$\rightarrow (5p^2 6d)\ ^2D_{3/2}$	$\rightarrow (5s^2 6d)\ ^2D_{5/2}$	$\rightarrow (5s^2 4f)\ ^2F_{7/2}$	$\rightarrow (5s^2 4f)\ ^2F_{5/2}$	$\rightarrow (5p^2 8s)\ ^2S_{1/2}$	$\rightarrow (5s^2 8p)\ ^2P_{1/2}$	$\rightarrow (5s^2 7d)\ ^2D_{3/2}$	$\rightarrow (5P^2 7d)\ ^2D_{5/2}$	$\rightarrow (5s^2 8p)\ ^2P_{3/2}$
23.8	0.0554	0.239	0.0315	0.0168	0.108	0.0302	0.0209	0.0465	0.0144	0.0228
24.9	0.0535	0.240	0.0309	0.0158	0.105	0.0307	0.0207	0.0457	0.0140	0.0221
26.3	0.0513	0.243	0.0301	0.0145	0.101	0.0313	0.0208	0.0447	0.0129	0.0212
27.3	0.0495	0.245	0.0293	0.0136	0.0975	0.0317	0.0209	0.0446	0.0125	0.0206
28.7	0.0476	0.246	0.0282	0.0126	0.0936	0.0322	0.0215	0.0448	0.0121	0.0202
30.1	0.0454	0.248	0.0271	0.0116	0.0897	0.0325	0.0213	0.0447	0.0113	0.0193
31.4	0.0434	0.249	0.0265	0.0108	0.0865	0.0329	0.0216	0.0450	0.0110	0.0184
32.8	0.0416	0.250	0.0257	0.0101	0.0833	0.0332	0.0216	0.0451	0.0106	0.0177
34.2	0.0399	0.251	0.0251	0.00943	0.0803	0.0334	0.0219	0.0452	0.0102	0.0170
35.8	0.0379	0.251	0.0243	0.00874	0.0768	0.0337	0.0222	0.0452	0.00979	0.0162
37.1	0.0363	0.251	0.0236	0.00823	0.0741	0.0337	0.0222	0.0451	0.00948	0.0156
38.8	0.0345	0.250	0.0228	0.00769	0.0711	0.0338	0.0225	0.0449	0.00913	0.0148
40.4	0.0328	0.248	0.0219	0.00720	0.0683	0.0337	0.0225	0.0445	0.00878	0.0141
42.0	0.0312	0.246	0.0212	0.00677	0.0657	0.0336	0.0224	0.0441	0.00848	0.0134
43.4	0.0300	0.245	0.0207	0.00644	0.0637	0.0336	0.0218	0.0436	0.00823	0.0129
45.0	0.0286	0.242	0.0201	0.00609	0.0615	0.0334	0.0218	0.0431	0.00796	0.0123
46.4	0.0275	0.240	0.0196	0.00584	0.0598	0.0332	0.0214	0.0426	0.00776	0.0118
48.0	0.0263	0.238	0.0190	0.00554	0.0578	0.0329	0.0212	0.0421	0.00751	0.0113
50.2	0.0248	0.235	0.0184	0.00519	0.0554	0.0325	0.0208	0.0415	0.00723	0.0107
52.1	0.0237	0.232	0.0178	0.00492	0.0535	0.0321	0.0203	0.0409	0.00700	0.0102
54.3	0.0225	0.229	0.0173	0.00464	0.0514	0.0316	0.0197	0.0402	0.00677	0.00966
55.6	0.0218	0.227	0.0170	0.00449	0.0503	0.0313	0.0194	0.0398	0.00665	0.00936
56.7	0.0213	0.225	0.0167	0.00437	0.0494	0.0311	0.0191	0.0395	0.00652	0.00913
57.8	0.0208	0.224	0.0165	0.00426	0.0485	0.0308	0.0188	0.0391	0.00645	0.00891
60.0	0.0198	0.220	0.0160	0.00404	0.0469	0.0303	0.0182	0.0385	0.00627	0.00850
65.0	0.0180	0.213	0.0151	0.00363	0.0438	0.0290	0.0170	0.0371	0.00589	0.00770
70.0	0.0165	0.206	0.0143	0.00330	0.0413	0.0278	0.0159	0.0357	0.00558	0.00703
75.0	0.0152	0.199	0.0137	0.00302	0.0393	0.0266	0.0150	0.0343	0.00533	0.00647
80.0	0.0142	0.192	0.0130	0.00279	0.0378	0.0255	0.0141	0.0329	0.00509	0.00601
85.0	0.0133	0.186	0.0125	0.00259	0.0367	0.0244	0.0134	0.0316	0.00487	0.00562
90.0	0.0126	0.180	0.0119	0.00242	0.0356	0.0234	0.0128	0.0305	0.00466	0.00529
95.0	0.0121	0.175	0.0114	0.00228	0.0345	0.0224	0.0122	0.0294	0.00447	0.00503
100	0.0117	0.170	0.0110	0.00216	0.0334	0.0215	0.0117	0.0283	0.00429	0.00482
105	0.0115	0.165	0.0106	0.00206	0.0324	0.0207	0.0113	0.0273	0.00414	0.00466
110	0.0114	0.161	0.0102	0.00197	0.0315	0.0200	0.0109	0.0264	0.00399	0.00455
115	0.0116	0.158	0.00979	0.00189	0.0306	0.0193	0.0106	0.0257	0.00384	0.00449

Journal of Physical and Chemical Reference Data
ARTICLE
scitation.org/journal/jpr

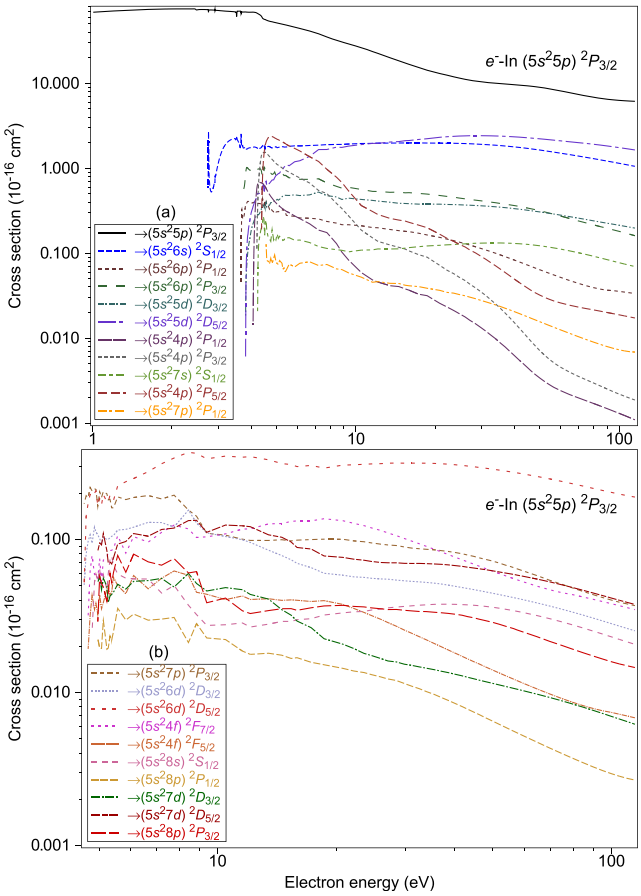

FIG. 4. Individual discrete inelastic cross sections ($\times 10^{-16}$ cm^2) for electron impact excitation of In from the $(5s^25p)\ ^2P_{3/2}$ metastable state to the higher-lying excited states as denoted in legends (a) and (b). All results are from our DBSR-214 calculation, and they represent our recommended data for each of these processes.

threshold up to 100 eV and from 100 eV up to 10 000 eV we, as in Sec. 3.1, making use of a suitably scaled RCCC-75 cross section (scaling factor = 0.7694) to facilitate the extrapolation to those higher energies and maintain continuity at 100 eV. We believe that the uncertainty estimate on this recommended ICS (again see Table 2) is ~±20%.

Given our discussion immediately above, it is no surprise that for the individual discrete inelastic transitions, from both the ground-state $(5s^25p)^2P_{1/2}$ level and the close-lying metastable $(5s^25p)^2P_{3/2}$ level, we have chosen to utilize our DBSR-214 calculations. Angle-ICSs for transitions from $(5s^25p)^2P_{1/2}$ to a higher lying level i, ICS$_i$, are plotted in Figs. 3(a) and 3(b) and listed in the corresponding Tables 3 and 4. A total of 21 discrete inelastic cross sections are presented here for the first time. Similarly, angle-ICSs from the $(5s^25p)^2P_{3/2}$ state to a higher level i are plotted in Figs. 4(a) and 4(b) and listed in the corresponding Tables 5 and 6. A further 21 discrete inelastic channels for excitation from the $(5s^25p)^2P_{3/2}$ are also presented here for the first time. Near-threshold structures are observed in most of these inelastic ICS$_i$ (see Figs. 3 and 4). These structures are not pseudo-resonances; rather, they either originate from Feshbach resonances or are associated with the opening of higher-lying discrete electronic states (possibly Wigner cusps) as the incident electron energy is increased. Nonetheless, a more detailed study of these structures, beyond the scope of this paper, is required before any quantitative classifications can be made. We believe the errors on these ICS$_i$, on average, are ±15% for transitions originating from the ground $(5s^25p)^2P_{1/2}$ state and ~±20% for those transitions originating from the metastable $(5s^25p)^2P_{3/2}$ state. Note that the $(5s^25p)^2P_{3/2}$ ICS$_i$s have been included here as we believe they will be needed in any quantitative kinetic-radiative study for a plasma in which indium is a constituent and may also be needed for our electron transport simulations in Sec. 4.

While we do not explicitly show our extrapolations for each ICS$_i$ out to 10 000 eV, such extrapolations are simple enough to undertake. If we again pick our RCCC-75 summed inelastic ICS to perform the extrapolation, and again do the normalization at 100 eV, then for all $E \geqslant 100$ eV, we find

$$\mathrm{ICS}_i(E) = \frac{\mathrm{ICS}_i(100\ \mathrm{eV})}{\mathrm{ICS}_{\mathrm{summed}}(100\ \mathrm{eV})} \times \mathrm{ICS}_{\mathrm{summed}}(E), \qquad (3)$$

where all the values for the right-hand side of Eq. (3) can be obtained from Tables 2–6 as required.

3.3. Total ionization cross section

In Fig. 5, we plot the available TICS for the scattering process $e^- + \mathrm{In} \rightarrow \mathrm{In}^+ + 2e^-$, including our present OP1, OP2, BEB, BEB+autoionization, RCCC-75, and DBSR-214 cross sections. It should be apparent that two experimental determinations, from Vainshtein *et al.*[12] and Shul *et al.*,[14] are available and that they disagree with one another (outside their reported uncertainties of ±18% and ±13%, respectively) in terms of their magnitudes. Vainshtein *et al.*[12] determined the number density of their indium beam using the quartz crystal resonator method, which Lindsay and Mangan[44] noted can lead to problematic results. Shul *et al.*,[14] however, employed a different approach that incorporates a fast neutral atom beam obtained by charge transfer of an energetic ion beam that is crossed by an ionizing electron beam. Unfortunately, as also noted by Lindsay and Mangan,[44] this approach does present formidable practical difficulties including being able to precisely ascertain the overlap between the electron beam and the fast neutral beam and with the possible presence of metastable species. Given the caveats in applying both those experimental procedures, we *a priori* have no way of choosing between them. From a theoretical perspective, we find that our RCCC-75 TICS underestimates the magnitude of all the other TICS results. This can be understood by the fact that it currently does not incorporate many of the important autoionization channels that Kim and Stone[18] noted are crucial to consider in this case. The semi-empirical calculation of Lotz[15] and the present BEB results favor the measurement of Vainshtein *et al.*,[12] while the present BEB+PWB autoionization, the corresponding calculation from the work of Kim and Stone,[18] and the electron impact total single ionization (EITSI) results[16] favor the experiment of Shul *et al.*[14] Finally, in between (but outside their stated measurement uncertainties) the experimental results, we find in Fig. 5 the present OP1, OP2, and DBSR-214 calculations and the Deutsch–Märk[17] computation. Note that, in principle, our OP1 and OP2 computations include those important autoionizing channels, while our DBSR-214 calculations incorporate most of them except for those that originate from the 4*d* shell.

Published by AIP Publishing on behalf of the National Institute of Standards and Technology.

TABLE 5. Angle-ICSs (10^{-16} cm^2) for electron–indium scattering from the ($5s^25p$) $^2P_{3/2}$ metastable state. See also supplementary material, Table S4a

	Cross section (10^{-16} cm^2)									
Energy (eV)	→ ($5s^25p$) $^2P_{3/2}$	→ ($5s^26s$) $^2S_{1/2}$	→ ($5s^26p$) $^2P_{1/2}$	→ ($5s^26p$) $^2P_{3/2}$	→ ($5s^25d$) $^2D_{3/2}$	→ ($5s^25d$) $^2D_{5/2}$	→ ($5s^24p$) $^2P_{1/2}$	→ ($5s^24p$) $^2P_{3/2}$	→ ($5s^27s$) $^2S_{1/2}$	→ ($5s^24p$) $^2P_{5/2}$	→ ($5s^27p$) $^2P_{1/2}$
1.005	68.7										
1.127	70.2										
1.290	71.9										
1.399	72.8										
1.562	73.8										
1.767	74.6										
1.903	75.0										
2.079	75.2										
2.365	75.2										
2.474	73.2										
2.748	72.6	0.00									
2.753	69.3	2.71									
2.757	71.8	1.67									
2.761	72.5	1.14									
2.767	72.8	0.873									
2.787	73.1	0.597									
2.814	73.1	0.528									
2.912	74.4	0.674									
2.915	71.3	0.817									
3.154	71.0	1.79									
3.522	61.2	2.36									
3.636	70.8	1.75									
3.655	69.8	2.04									
3.660	69.2	2.54									
3.670	68.8	2.41	0.00								
3.674	69.1	1.92	0.208								
3.677	69.3	1.82	0.295								
3.685	69.4	1.79	0.329								
3.707	69.0	1.85	0.263	0.00							
3.712	68.8	1.85	0.254	0.463							
3.804	69.1	1.77	0.362	0.818	0.00						
3.807	69.1	1.77	0.368	0.838	0.0142	0.00					
3.807	69.1	1.77	0.369	0.843	0.0176	0.00596					
3.821	69.1	1.70	0.367	0.943	0.0451	0.0520					
3.875	68.8	1.70	0.406	1.01	0.0978	0.160					
4.062	68.8	1.77	0.394	0.933	0.221	0.351	0.00				
4.066	68.8	1.77	0.394	0.932	0.223	0.355	0.0143				
4.093	68.7	1.78	0.397	0.953	0.236	0.377	0.0980				
4.192	67.5	1.75	0.403	1.00	0.279	0.456	0.540	0.00			
4.202	67.2	1.75	0.403	0.999	0.285	0.461	0.580	0.106			
4.227	66.5	1.69	0.391	0.989	0.287	0.499	0.643	0.311	0.00		
4.229	66.5	1.68	0.389	0.987	0.287	0.503	0.648	0.334	0.0204		
4.256	65.7	1.68	0.385	0.978	0.283	0.503	0.678	0.577	0.107		
4.369	61.9	1.76	0.370	0.935	0.330	0.551	0.675	1.39	0.197	0.00	
4.392	60.4	1.80	0.344	0.838	0.337	0.583	0.670	1.49	0.208	0.424	

TABLE 5. (*Continued.*)

	Cross section (10^{-16} cm^2)										
Energy (eV)	$\rightarrow (5s^2 5p)\ ^2P_{3/2}$	$\rightarrow (5s^2 6s)\ ^2S_{1/2}$	$\rightarrow (5s^2 6p)\ ^2P_{1/2}$	$\rightarrow (5s^2 6p)\ ^2P_{3/2}$	$\rightarrow (5s^2 5d)\ ^2D_{3/2}$	$\rightarrow (5s^2 5d)\ ^2D_{5/2}$	$\rightarrow (5s^2 4p)\ ^2P_{1/2}$	$\rightarrow (5s^2 4p)\ ^2P_{3/2}$	$\rightarrow (5s^2 7s)\ ^2S_{1/2}$	$\rightarrow (5s^2 4p)\ ^2P_{5/2}$	$\rightarrow (5s^2 7p)\ ^2P_{1/2}$
4.420	58.3	1.85	0.437	1.05	0.353	0.609	0.660	1.51	0.232	0.835	
4.474	56.9	1.74	0.389	0.946	0.359	0.540	0.635	1.54	0.246	1.49	
4.501	56.5	1.72	0.404	1.01	0.350	0.574	0.611	1.52	0.163	1.70	
4.544	55.9	1.77	0.409	0.934	0.384	0.684	0.590	1.53	0.238	1.98	0.00
4.556	55.6	1.76	0.428	0.934	0.397	0.698	0.581	1.52	0.244	2.04	0.127
4.583	55.2	1.79	0.364	0.888	0.350	0.628	0.558	1.49	0.187	2.14	0.0820
4.692	53.8	1.80	0.329	0.867	0.366	0.664	0.491	1.38	0.148	2.35	0.0746
4.746	53.4	1.76	0.343	0.873	0.394	0.695	0.466	1.32	0.138	2.38	0.0872
4.801	53.0	1.74	0.318	0.846	0.394	0.726	0.445	1.27	0.188	2.36	0.0759
4.869	52.4	1.75	0.307	0.863	0.399	0.731	0.420	1.21	0.143	2.32	0.0874
5.018	51.3	1.74	0.307	0.819	0.430	0.839	0.377	1.11	0.168	2.19	0.0754
5.236	49.8	1.78	0.317	0.843	0.462	0.979	0.337	1.01	0.149	2.06	0.0761
5.386	48.8	1.78	0.304	0.826	0.481	1.06	0.318	0.956	0.153	1.96	0.0601
5.576	47.6	1.81	0.275	0.771	0.478	1.07	0.299	0.898	0.152	1.83	0.0744
5.848	45.9	1.84	0.272	0.774	0.486	1.19	0.275	0.827	0.142	1.71	0.0689
6.66	41.3	1.85	0.258	0.740	0.486	1.38	0.222	0.670	0.133	1.37	0.0792
7.21	38.3	1.87	0.253	0.751	0.524	1.66	0.187	0.547	0.120	1.20	0.0715
7.75	35.1	1.90	0.236	0.671	0.476	1.66	0.175	0.504	0.114	0.972	0.0736
8.84	30.7	1.91	0.216	0.583	0.429	1.76	0.103	0.335	0.108	0.679	0.0641
9.39	29.1	1.93	0.216	0.595	0.444	1.82	0.0827	0.274	0.104	0.538	0.0585
10.5	26.2	1.96	0.210	0.562	0.429	1.90	0.0593	0.187	0.109	0.364	0.0522
11.6	23.6	1.96	0.200	0.534	0.418	1.96	0.0484	0.151	0.109	0.309	0.0454
12.1	22.5	1.97	0.199	0.532	0.411	1.96	0.0457	0.138	0.112	0.286	0.0463
13.5	20.0	1.98	0.190	0.521	0.398	2.04	0.0414	0.125	0.112	0.257	0.0442
15.4	17.3	1.99	0.181	0.514	0.385	2.11	0.0380	0.112	0.115	0.239	0.0419
17.3	15.4	1.99	0.172	0.506	0.378	2.18	0.0329	0.0962	0.119	0.214	0.0404
18.6	14.3	1.98	0.164	0.496	0.378	2.23	0.0316	0.0897	0.122	0.199	0.0386
20.8	13.0	1.98	0.153	0.478	0.378	2.32	0.0257	0.0718	0.124	0.167	0.0365
22.2	12.5	1.97	0.146	0.466	0.374	2.35	0.0233	0.0630	0.125	0.150	0.0345
24.6	11.5	1.96	0.135	0.446	0.372	2.39	0.0195	0.0522	0.128	0.128	0.0326
27.1	10.9	1.94	0.125	0.428	0.367	2.41	0.0162	0.0432	0.130	0.109	0.0304
29.8	10.4	1.91	0.114	0.414	0.361	2.42	0.0133	0.0352	0.131	0.0922	0.0278
32.5	10.1	1.88	0.104	0.399	0.355	2.41	0.0109	0.0283	0.132	0.0774	0.0256
35.5	9.89	1.85	0.0949	0.384	0.347	2.39	0.00867	0.0221	0.132	0.0643	0.0234
38.5	9.71	1.80	0.0866	0.370	0.339	2.36	0.00694	0.0172	0.131	0.0538	0.0214
41.8	9.53	1.76	0.0788	0.355	0.329	2.32	0.00548	0.0131	0.129	0.0450	0.0194
44.8	9.34	1.71	0.0726	0.340	0.321	2.29	0.00452	0.0103	0.127	0.0390	0.0179
49.9	8.98	1.64	0.0638	0.316	0.306	2.22	0.00339	0.00712	0.122	0.0321	0.0156
57.5	8.34	1.53	0.0542	0.283	0.286	2.13	0.00256	0.00491	0.114	0.0269	0.0131
64.7	7.77	1.45	0.0477	0.257	0.269	2.05	0.00217	0.00398	0.107	0.0244	0.0114
69.7	7.40	1.39	0.0443	0.240	0.259	2.00	0.00199	0.00356	0.101	0.0232	0.0104
79.7	6.87	1.30	0.0393	0.216	0.241	1.92	0.00170	0.00297	0.0921	0.0215	0.00899
89.7	6.51	1.22	0.0367	0.196	0.226	1.83	0.00148	0.00253	0.0841	0.0201	0.00797
99.7	6.30	1.14	0.0355	0.181	0.213	1.75	0.00130	0.00220	0.0774	0.0188	0.00729
115	6.14	1.05	0.0335	0.161	0.197	1.64	0.00109	0.00187	0.0696	0.0173	0.00685

Journal of Physical and Chemical Reference Data
ARTICLE
scitation.org/journal/jpr

TABLE 6. Angle-ICSs (10^{-16} cm^2) for electron–indium scattering from the $5p_{3/2}$ metastable state. See also supplementary material, Table S4b

Energy	Cross section (10^{-16} cm^2)									
	$\rightarrow (5s^2 7p)\ ^2P_{3/2}$		$\rightarrow (5s^2 6d)\ ^2D_{5/2}$		$\rightarrow (5s^2 4f)\ ^2F_{5/2}$		$\rightarrow (5s^2 8p)\ ^2P_{1/2}$		$\rightarrow (5p^2 7d)\ ^2D_{5/2}$	
Energy (eV)		$\rightarrow (5p^2 6d)\ ^2D_{3/2}$		$\rightarrow (5s^2 4f)\ ^2F_{7/2}$		$\rightarrow (5p^2 8s)\ ^2S_{1/2}$		$\rightarrow (5s^2 7d)\ ^2D_{3/2}$		$\rightarrow (5s^2 8p)\ ^2P_{3/2}$
4.558	0.00									
4.567	0.0635	0.00								
4.573	0.105	0.0194	0.00							
4.583	0.170	0.0496	0.0490							
4.637	0.192	0.0800	0.142							
4.649	0.191	0.0836	0.148	0.00	0.00					
4.692	0.187	0.0968	0.172	0.0314	0.0192					
4.746	0.218	0.107	0.196	0.0616	0.0317					
4.764	0.214	0.103	0.194	0.0671	0.0354	0.00				
4.801	0.206	0.0938	0.189	0.0784	0.0430	0.0247				
4.869	0.214	0.120	0.200	0.0588	0.0346	0.0524				
4.909	0.211	0.112	0.207	0.0600	0.0381	0.0592				
4.912	0.209	0.111	0.205	0.0598	0.0379	0.0589	0.00			
4.913	0.208	0.111	0.204	0.0597	0.0377	0.0588	4.94×10^{-4}	0.00		
4.916	0.205	0.111	0.202	0.0595	0.0374	0.0584	0.00185	0.00324	0.00	
4.918	0.203	0.111	0.200	0.0593	0.0371	0.0582	0.00288	0.00571	0.00421	0.00
4.964	0.164	0.107	0.166	0.0556	0.0322	0.0531	0.0224	0.0522	0.0835	0.0290
5.018	0.204	0.101	0.184	0.0745	0.0432	0.0640	0.0194	0.0569	0.0944	0.0572
5.073	0.187	0.0935	0.167	0.0529	0.0350	0.0472	0.0193	0.0466	0.0917	0.0512
5.127	0.205	0.103	0.196	0.0729	0.0385	0.0585	0.0295	0.0555	0.109	0.0487
5.236	0.198	0.0994	0.175	0.0761	0.0472	0.0467	0.0191	0.0491	0.0837	0.0392
5.277	0.181	0.0998	0.177	0.0822	0.0496	0.0594	0.0194	0.0386	0.0702	0.0443
5.331	0.182	0.102	0.193	0.0842	0.0430	0.0736	0.0233	0.0424	0.0708	0.0599
5.386	0.160	0.104	0.186	0.0846	0.0454	0.0776	0.0220	0.0435	0.0688	0.0520
5.440	0.160	0.105	0.179	0.0863	0.0562	0.0674	0.0248	0.0449	0.0754	0.0605
5.576	0.189	0.115	0.223	0.105	0.0498	0.0592	0.0353	0.0507	0.0927	0.0783
5.848	0.181	0.116	0.237	0.0810	0.0440	0.0555	0.0296	0.0471	0.0965	0.0607
6.12	0.187	0.120	0.249	0.104	0.0578	0.0550	0.0324	0.0530	0.109	0.0798
6.66	0.193	0.129	0.276	0.0956	0.0474	0.0548	0.0295	0.0536	0.105	0.0711
7.21	0.183	0.128	0.311	0.111	0.0555	0.0444	0.0300	0.0554	0.116	0.0676
7.75	0.194	0.120	0.339	0.123	0.0619	0.0499	0.0308	0.0486	0.118	0.0746
8.43	0.155	0.155	0.369	0.117	0.0581	0.0370	0.0211	0.0597	0.132	0.0601
8.84	0.141	0.127	0.364	0.102	0.0449	0.0321	0.0281	0.0513	0.133	0.0613
9.39	0.109	0.110	0.335	0.104	0.0436	0.0273	0.0226	0.0458	0.111	0.0384
10.5	0.106	0.104	0.349	0.108	0.0403	0.0276	0.0221	0.0482	0.124	0.0412
11.6	0.0999	0.0991	0.343	0.116	0.0425	0.0283	0.0186	0.0467	0.122	0.0340
12.1	0.0981	0.0952	0.346	0.117	0.0403	0.0266	0.0177	0.0435	0.121	0.0326
13.5	0.0980	0.0847	0.330	0.126	0.0408	0.0278	0.0180	0.0406	0.107	0.0341
14.6	0.0991	0.0781	0.312	0.126	0.0398	0.0290	0.0174	0.0346	0.103	0.0351
15.4	0.0974	0.0733	0.307	0.130	0.0401	0.0290	0.0166	0.0318	0.0958	0.0351
15.9	0.0985	0.0695	0.298	0.132	0.0399	0.0298	0.0168	0.0291	0.0882	0.0343
17.3	0.0993	0.0651	0.303	0.132	0.0391	0.0302	0.0157	0.0264	0.0862	0.0356
18.6	0.0999	0.0598	0.291	0.136	0.0396	0.0319	0.0151	0.0223	0.0776	0.0366
20.8	0.0998	0.0581	0.305	0.132	0.0374	0.0330	0.0143	0.0206	0.0760	0.0369
22.2	0.0974	0.0567	0.306	0.127	0.0352	0.0335	0.0137	0.0193	0.0739	0.0363

TABLE 6. (*Continued.*)

Energy	Cross section (10^{-16} cm^2)									
	→ $(5s^2 7p)\ ^2P_{3/2}$	→ $(5p^2 6d)\ ^2D_{3/2}$	→ $(5s^2 6d)\ ^2D_{5/2}$	→ $(5s^2 4f)\ ^2F_{7/2}$	→ $(5s^2 4f)\ ^2F_{5/2}$	→ $(5p^2 8s)\ ^2S_{1/2}$	→ $(5s^2 8p)\ ^2P_{1/2}$	→ $(5s^2 7d)\ ^2D_{3/2}$	→ $(5p^2 7d)\ ^2D_{5/2}$	→ $(5s^2 8p)\ ^2P_{3/2}$
Energy (eV)										
23.5	0.0961	0.0562	0.308	0.122	0.0332	0.0337	0.0134	0.0179	0.0728	0.0361
24.6	0.0944	0.0555	0.310	0.118	0.0316	0.0344	0.0130	0.0173	0.0714	0.0355
26.0	0.0927	0.0549	0.311	0.114	0.0299	0.0349	0.0126	0.0166	0.0704	0.0351
27.1	0.0916	0.0547	0.313	0.110	0.0285	0.0355	0.0122	0.0160	0.0701	0.0347
28.4	0.0908	0.0540	0.314	0.105	0.0270	0.0360	0.0119	0.0158	0.0700	0.0347
29.8	0.0889	0.0534	0.314	0.101	0.0255	0.0363	0.0114	0.0152	0.0695	0.0343
31.2	0.0873	0.0529	0.314	0.0970	0.0242	0.0367	0.0109	0.0150	0.0694	0.0340
32.5	0.0865	0.0526	0.314	0.0933	0.0231	0.0370	0.0105	0.0146	0.0694	0.0337
33.9	0.0858	0.0521	0.314	0.0898	0.0220	0.0372	0.0101	0.0143	0.0692	0.0336
35.5	0.0852	0.0516	0.312	0.0858	0.0208	0.0375	0.00966	0.0140	0.0688	0.0333
36.9	0.0842	0.0510	0.311	0.0828	0.0199	0.0375	0.00926	0.0137	0.0685	0.0330
38.5	0.0831	0.0501	0.309	0.0793	0.0189	0.0376	0.00884	0.0134	0.0679	0.0327
40.1	0.0818	0.0492	0.306	0.0762	0.0180	0.0375	0.00843	0.0131	0.0671	0.0323
41.8	0.0803	0.0483	0.303	0.0733	0.0171	0.0373	0.00805	0.0128	0.0664	0.0318
43.1	0.0787	0.0476	0.300	0.0711	0.0165	0.0372	0.00774	0.0125	0.0655	0.0312
44.8	0.0771	0.0468	0.297	0.0685	0.0158	0.0370	0.00740	0.0122	0.0647	0.0306
46.1	0.0755	0.0461	0.294	0.0666	0.0153	0.0367	0.00714	0.0120	0.0640	0.0300
47.8	0.0739	0.0453	0.291	0.0644	0.0147	0.0364	0.00683	0.0117	0.0632	0.0294
49.9	0.0719	0.0443	0.287	0.0618	0.0139	0.0359	0.00647	0.0114	0.0621	0.0286
51.8	0.0699	0.0434	0.283	0.0597	0.0134	0.0354	0.00617	0.0112	0.0611	0.0278
54.0	0.0674	0.0425	0.278	0.0575	0.0128	0.0348	0.00587	0.0109	0.0599	0.0269
55.4	0.0662	0.0419	0.275	0.0562	0.0124	0.0344	0.00569	0.0107	0.0593	0.0264
56.5	0.0651	0.0415	0.273	0.0552	0.0122	0.0341	0.00556	0.0106	0.0588	0.0260
57.5	0.0640	0.0410	0.271	0.0543	0.0119	0.0338	0.00543	0.0105	0.0582	0.0255
59.7	0.0620	0.0402	0.267	0.0526	0.0114	0.0331	0.00519	0.0102	0.0572	0.0247
64.7	0.0578	0.0383	0.257	0.0493	0.0105	0.0317	0.00471	0.00971	0.0548	0.0230
69.7	0.0538	0.0365	0.248	0.0467	0.00973	0.0302	0.00431	0.00923	0.0526	0.0215
74.7	0.0508	0.0349	0.238	0.0447	0.00910	0.0288	0.00398	0.00879	0.0504	0.0202
79.7	0.0479	0.0333	0.230	0.0434	0.00858	0.0275	0.00370	0.00837	0.0483	0.0191
84.7	0.0455	0.0319	0.222	0.0419	0.00816	0.0263	0.00346	0.00798	0.0463	0.0181
89.7	0.0434	0.0305	0.215	0.0405	0.00783	0.0251	0.00325	0.00762	0.0445	0.0172
94.7	0.0416	0.0293	0.208	0.0391	0.00757	0.0240	0.00308	0.00728	0.0428	0.0165
99.7	0.0400	0.0281	0.202	0.0379	0.00738	0.0230	0.00294	0.00696	0.0413	0.0158
105	0.0387	0.0270	0.197	0.0367	0.00718	0.0221	0.00282	0.00668	0.0398	0.0153
110	0.0377	0.0261	0.192	0.0356	0.00698	0.0213	0.00273	0.00642	0.0386	0.0149
115	0.0368	0.0252	0.188	0.0346	0.00680	0.0205	0.00266	0.00617	0.0374	0.0145

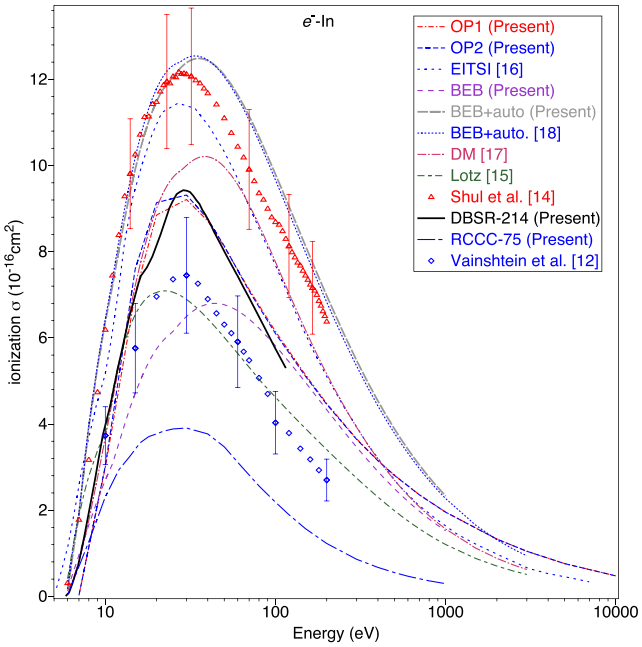

FIG. 5. TICSs ($\times 10^{-16}$ cm^2) for the process $e^- + \text{In} \rightarrow \text{In}^+ + 2e^-$. Experimental data from the work of Vainshtein *et al.*[12] (blue diamonds) and Shul *et al.*[14] (red triangles) are plotted, along with earlier theoretical results from the work of Lotz[15] (green dotted-dashed line), an EITSI calculation[16] (blue dashed line), a Deutsch–Märk computation[17] (magenta dotted-dashed line), and a BEB+PWB calculation[18] (blue dotted line). Also plotted are our current BEB result (purple dashed line), OP1 (red dotted-dashed line) and OP2 (blue dashed line) results, RCCC-75 (blue dotted-dashed line) calculation, BEB+PWB (gray dashed line) calculation, and DBSR-214 (black solid line) computation. See also the legend in the figure.

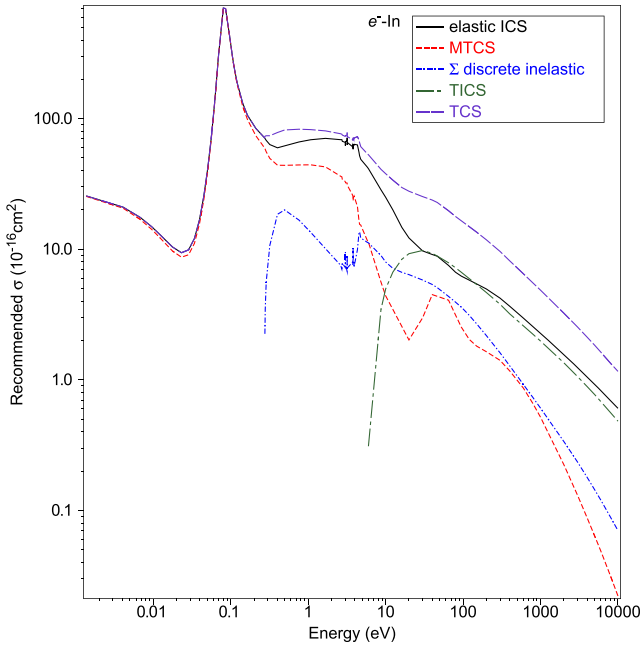

FIG. 6. Summary plot showing our recommended electron–In cross sections ($\times 10^{-16}$ cm^2) for elastic scattering, the sum over all discrete inelastic cross sections, the TICS, and the grand total cross section. See also the legend in the figure.

Given the discussion above, it appears reasonable to assert that the measurements from the work of Vainshtein *et al.*[12] can constitute a lower bound on the true TICS, while those from the work of Shul *et al.*[14] can be considered as an upper bound. In the latter case, this seems reasonable, as it is well known that PWB based calculations, without some appropriate scaling,[5] will overestimate the magnitude of the cross sections they calculate so that the BEB+PWB autoionization cross-section magnitude should also be too large. Under these circumstances, when coming to form a recommended TICS database, we will follow the approach of Itikawa (see e.g., Ref. 45), which essentially means that for energies from threshold to 200 eV, we take an average of the available experimental data, and then from 200 eV to 10 000 eV, we use a suitably scaled (scaling factor = 1.014) OP1 result to effect the extrapolation to higher energies. Note that we have had to employ Itikawa's method (successfully) in some of our recent data compilations for electron scattering from some other atomic species.[19,20,46] The estimated uncertainty on this is ~±22%, reflecting the error carried forward in taking the average of the TICS measurements.[12,14] Interestingly, this recommended TICS, to within our error just cited, is in quite good accord with the results from our OP1, OP2, and DBSR-214 calculations. The present recommended TICS can be found in Table 2, and they are also plotted in Fig. 6 along with our recommended elastic ICS, MTCS, and sum over all discrete inelastic angle-ICSs.

3.4. TCS

The recommended TCS for E_0 = 0.001 eV–10 000 eV is now simply formed by, at each incident electron energy, adding up the results for the recommended elastic ICS, the recommended sum over all discrete inelastic excitation ICS, and the recommended TICS, namely, summing up the results of columns 1, 3, and 4 of Table 2. That recommended TCS can also now be found in column 5 of Table 2, as well as being plotted in Fig. 6.

4. Simulated Transport Coefficients

In what follows, we implement a well-benchmarked multi-term solution of Boltzmann's equation[2,47,48] for the calculation of electron swarm transport coefficients in gaseous In over a range of reduced electric fields E/n_0, varying from 10^{-2} Td to 10^4 Td, where 1 Td = 1 Townsend = 10^{-21} V m^2 and n_0 is the neutral number density. The two-term approximation (TTA)[47,48] tends to break down at the higher E/n_0 considered, although it remains accurate to within 20% for all transport coefficients, with the exception of some of the diffusion coefficients. Under the TTA at high E/n_0, these errors in diffusion can be as large as 51% for the flux transverse diffusion coefficient, 69% for the bulk longitudinal diffusion coefficient, and 70% for the flux longitudinal diffusion coefficient. In our calculations, we assume isotropic scattering in the excitation and ionization processes, while we have included the anisotropic nature of elastic scattering through the use of the elastic MTCSs. We consider transport through an In vapor at temperature T = 1260 K, which is in the vicinity of our previous crossed-beam experimental measurements.[1,9] As the corresponding thermal energy,

Published by AIP Publishing on behalf of the National Institute of Standards and Technology.

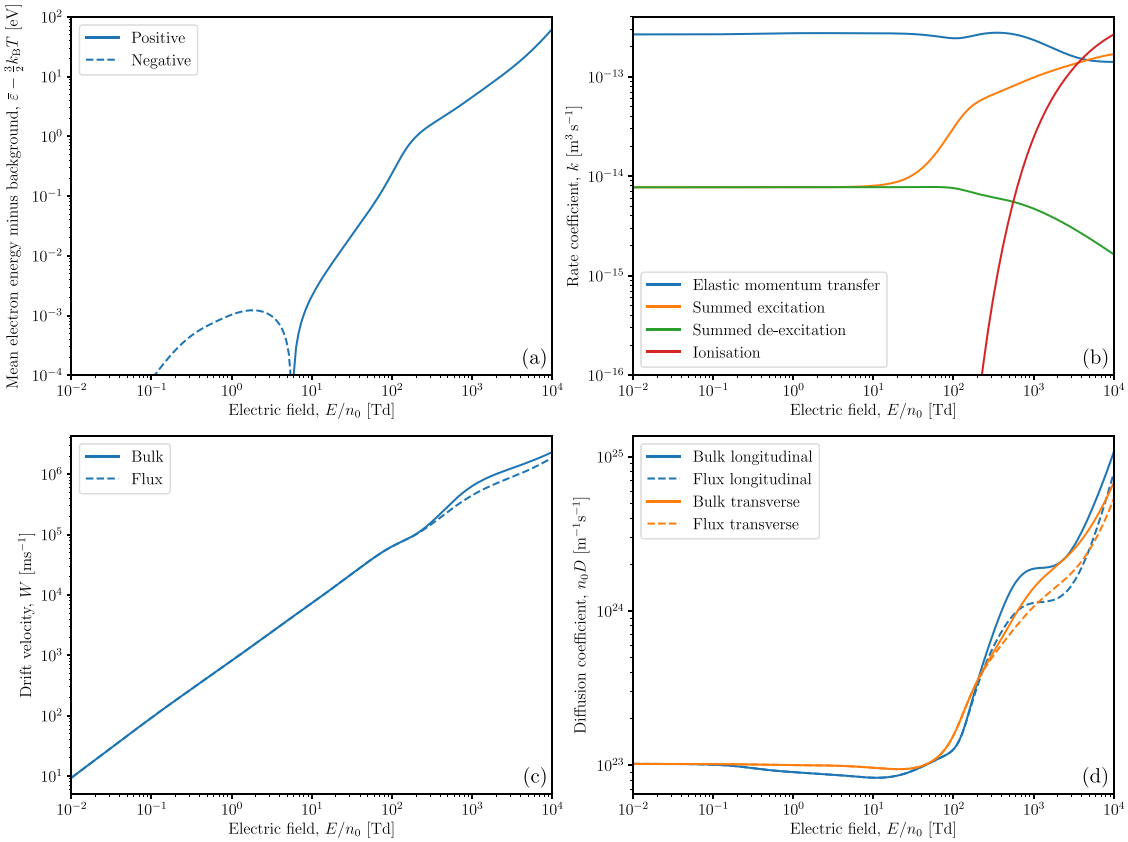

FIG. 7. Calculated mean electron energies (above the thermal background) (a), rate coefficients (b), drift velocities (c), and diffusion coefficients (d) for electrons in In vapor at temperature $T = 1260$ K (with thermal energy $\frac{3}{2}k_B T \approx 0.163$ eV) over a range of reduced electric fields. See also the legends for further details.

$\frac{3}{2}k_B T \approx 0.163$ eV, is on the order of the energy of the first $(5p)^2 P_{3/2}$ metastable state (~0.274 eV), we consider it prudent to account for de-excitation/superelastic collisions in our Boltzmann equation solution. Indeed, by applying Maxwell–Boltzmann statistics to In vapor at the aforementioned temperature, we determine that 86% of In atoms are in the ground state, with the remaining 14% almost exclusively in the first $(5p)^2 P_{3/2}$ metastable state. Note that we determine each de-excitation cross section from its corresponding excitation cross section by employing the principle of microscopic reversibility and detailed balancing.[49] We use our recommended elastic MTCS for elastic collisions with ground-state In atoms and obtain a separate elastic MTCS for In atoms in the first $(5p)^2 P_{3/2}$ metastable state by scaling our $(5p)^2 P_{3/2} \rightarrow (5p)^2 P_{3/2}$ elastic ICS by the ratio of our recommended elastic MTCS to recommended elastic ICS. Similarly, while we use our recommended TICS for ionization of In atoms in the ground state, we shift the energy threshold of our recommended TICS down to ~5.786 eV − 0.274 eV = 5.512 eV for ionization of In atoms already excited to the first $(5p)^2 P_{3/2}$ metastable state. The resulting calculated mean electron energies, rate coefficients, drift velocities, and diffusion coefficients are presented in Fig. 7. Figure 7(a) shows the difference between the mean electron energy $\bar{\varepsilon}$ and the thermal energy of the In vapor, $\frac{3}{2}k_B T \approx 0.163$ eV. In the low-field regime, near 10^{-2} Td, this energy difference is very small, indicating that the electrons are in thermal equilibrium with the background In atoms. As E/n_0 increases, the mean electron energy decreases, reaching a minimum of ~1 meV below the thermal background at ~1.8 Td. We attribute this cooling to be primarily due to the $(5p)^2 P_{1/2} \rightarrow (5p)^2 P_{3/2}$ transition, resulting in a greater power output from the swarm due to excitations than input from the electric field, superelastic collisions, and elastic collisions in this regime. Eventually, as E/n_0 approaches ~5.7 Td, the latter heating processes dominate enough to return the swarm to thermal equilibrium with the background. Then, as E/n_0 is increased further, the mean energy increases rapidly, slowing slightly in its ascent from ~200 Td onward due to the significant opening of the ionization channel. Figure 7(b) shows rate coefficients for elastic momentum transfer, summed excitation, summed de-excitation, and ionization processes. The elastic momentum transfer rate coefficient remains somewhat constant up to 1000 Td, before decreasing slightly at higher E/n_0. The summed excitation and de-excitation rate coefficients are identical close to thermal equilibrium, as is expected due to detailed balancing. These rate coefficients begin to depart visibly from 10 Td onward, with an increase in excitation events and decrease in de-excitation events. Although it should be noted that this departure starts much earlier than this as it is the slight excess of excitation events at low E/n_0 that is responsible for the ~1 meV cooling of electrons below the background. The ionization rate coefficient is zero in the low-field regime, before becoming appreciable around roughly 200 Td. In the high-field regime, near 10 000 Td, ionization dominates with its rate coefficient exceeding

those for all other processes. Figure 7(c) shows the bulk and flux drift velocities of the swarm, both of which are observed to increase monotonically with E/n_0, coinciding with one another up until the nonconservative effects of ionization manifest at around 200 Td. In the nonconservative regime from ~200 Td onward, the bulk drift velocity exceeds the flux, suggesting that electrons are being preferentially created at the front of the swarm, shifting the center of mass in the direction of the applied field. Figure 7(d) shows bulk and flux diffusion coefficients in the directions longitudinal and transverse to the applied electric field. Of course, below ~200 Td, the bulk and flux diffusion coefficients coincide. Below 0.1 Td, the transverse and longitudinal diffusion coefficients are essentially equal due to the expected isotropy of the electron velocity distribution in this regime. Above 0.1 Td, both diffusion coefficients begin to decrease slightly, reaching minima at roughly 10 Td and 20 Td for the longitudinal and transverse coefficients, respectively. Past these minima, both diffusion coefficients then proceed to rise monotonically with increasing E/n_0. In the nonconservative regime above ~200 Td, the bulk diffusion coefficients exceed their flux counterparts, suggesting a preferential creation of electrons at the sides of the swarm, in addition to its front.

5. Conclusions

We have compiled a complete angle-ICS database for electron–In scattering. As a part of that process, additional theoretical computations were undertaken, with these results also being reported here. While the need for having complete and accurate cross-section databases, for modeling a variety of electron-driven phenomena,[50,51] is now well understood, recent work from the Madrid group[52–54] has reinforced that assessment.

Interesting scattering results from this investigation include the very large shape resonances in the low-energy elastic ICS and MTCS, a series of near-threshold resonances in many of the discrete inelastic scattering channels we have considered, and the lack of consistent measurements for the experimental TICS in electron–In scattering. While there is no doubt that such experiments in In are difficult to undertake, further measurements of the TICS are clearly desirable.

Finally, we have employed our recommended cross sections to study the behavior of a swarm of electrons, drifting through a background gas of In, under the influence of an applied electric field. This analysis was undertaken using a multi-term Boltzmann equation solution to determine the relevant transport coefficients. Interesting results from this study included the need to allow for superelastic processes, the breakdown of the TTA in simulating the relevant transport coefficients in some regions of E/n_0, and that there was cooling in the mean electron energy of the swarm at ~1.8 Td, which can be associated with the opening of the $(5p)^2P_{3/2}$ metastable channel.

6. Supplementary Material

See the supplementary material for Excel tables of the present data.

Acknowledgments

The work of K.R.H., O.Z., and K.B. was supported by the United States National Science Foundation under Grant Nos. OAC-1834740 and PHY-1803844 and by the XSEDE supercomputer Allocation No. PHY-090031. The (D)BSR calculations were carried out on Stampede2 at the Texas Advanced Computing Center. The work of D.V.F. and I.B. was supported by the Australian Research Council and resources provided by the Pawsey Supercomputing Centre with funding from the Australian Government and the Government of Western Australia. F.B. and G.G. acknowledge partial financial support from the Spanish Ministry MICIU (Project Nos. FIS2016-80440 and PID2019-104727-RB-C21) and CSIC (Project No. LINKA20085). This work was also financially supported, in part, by the Australian Research Council (Project No. DP180101655), the Ministry of Education, Science and Technological Development of the Republic of Serbia, and the Institute of Physics (Belgrade).

7. Data Availability

The data that support the findings of this study are available from the corresponding author upon reasonable request.

8. References

[1]K. R. Hamilton, O. Zatsarinny, K. Bartschat, M. S. Rabasović, D. Šević, B. P. Marinković, S. Dujko, J. Atić, D. V. Fursa, I. Bray, R. P. McEachran, F. Blanco, G. García, P. W. Stokes, R. D. White, and M. J. Brunger, Phys. Rev. A **102**, 022801 (2020).

[2]R. D. White, D. Cocks, G. Boyle, M. Casey, N. Garland, D. Konovalov, B. Philippa, P. Stokes, J. de Urquijo, O. González-Magaña, R. P. McEachran, S. J. Buckman, M. J. Brunger, G. Garcia, S. Dujko, and Z. L. Petrovic, Plasma Sources Sci. Technol. **27**, 053001 (2018).

[3]J. de Urquijo, M. J. E. Casey, L. N. Serkovic-Loli, D. G. Cocks, G. J. Boyle, D. B. Jones, M. J. Brunger, and R. D. White, J. Chem. Phys. **151**, 054309 (2019).

[4]C. M. Ögün, W. Truong, C. Kaiser, R. Kling, and W. Heering, J. Phys. D: Appl. Phys. **47**, 285202 (2014).

[5]H. Tanaka, M. J. Brunger, L. Campbell, H. Kato, M. Hoshino, and A. R. P. Rau, Rev. Mod. Phys. **88**, 025004 (2016).

[6]L. C. Pitchford, L. L. Alves, K. Bartschat, S. F. Biagi, M.-C. Bordage, I. Bray, C. E. Brion, M. J. Brunger, L. Campbell *et al.*, Plasma Process. Polym. **14**, 1600098 (2017).

[7]R. S. M. Chrystile, I. S. Burns, J. Hult, and C. F. Kaminski, Opt. Lett. **34**, 2492 (2009).

[8]J. Hult, I. S. Burns, and C. F. Kaminski, Proc. Combust. Inst. **30**, 1535 (2005).

[9]M. S. Rabasović, V. I. Kelemen, S. D. Tošić, D. Šević, M. M. Dovhanych, V. Pejčev, D. M. Filipović, E. Yu Remeta, and B. P. Marinković, Phys. Rev. A **77**, 062713 (2008).

[10]M. Gryziński, Phys. Rev. **138**, A336 (1965).

[11]M. Gryziński, Phys. Rev. **138**, A322 (1965).

[12]L. A. Vainshtein, D. G. Golovach, V. I. Ochkur, V. I. Rakhovskiĭ, N. M. Rumyantsev, and V. M. Shustryakov, Sov. Phys. JETP **66**, 36 (1987).

[13]L. L. Shimon, E. I. Nepiipov, and I. P. Zapesochnyi, Sov. Phys. Tech. Phys. **20**, 434 (1975).

[14]R. J. Shul, R. C. Wetzel, and R. S. Freund, Phys. Rev. A **39**, 5588 (1989).

[15]W. Lotz, Z. Phys. A **232**, 101 (1970).

[16]M. R. Talukder, S. Bose, M. A. R. Patoary, A. K. F. Haque, M. A. Uddin, A. K. Basak, and M. Kando, Eur. Phys. J. D **46**, 281 (2008).

[17]D. Margreiter, H. Deutsch, and T. D. Märk, Int. J. Mass Spectrom. Ion Proc. **139**, 127 (1994).

[18]Y.-K. Kim and P. M. Stone, Phys. Rev. A **64**, 052707 (2001).

[19]R. P. McEachran, F. Blanco, G. García, and M. J. Brunger, J. Phys. Chem. Ref. Data **47**, 033103 (2018).

[20]R. P. McEachran, F. Blanco, G. García, P. W. Stokes, R. D. White, and M. J. Brunger, J. Phys. Chem. Ref. Data **47**, 043104 (2018).

[21]B. P. Marinković, R. Panajotović, D. Šević, R. P. McEachran, G. García, F. Blanco, and M. J. Brunger, Phys. Rev. A **99**, 062702 (2019).

[22]B. Predojević, D. Šević, B. P. Marinković, R. P. McEachran, F. Blanco, G. García, and M. J. Brunger, Phys. Rev. A **101**, 032704 (2020).
[23]R. D. Cowan, *The Theory of Atomic Structure and Spectra* (University of California Press, 1981).
[24]M. E. Riley and D. G. Truhlar, J. Chem. Phys. **63**, 2182 (1975).
[25]X. Zhang, J. Sun, and Y. Liu, J. Phys. B: At., Mol. Opt. Phys. **25**, 1893 (1992).
[26]R. P. McEachran, L. A. Parcell, and A. D. Stauffer, J. Phys. B: At., Mol. Opt. Phys. **28**, 2487 (1995).
[27]G. Staszewska, D. W. Schwenke, D. Thirumalai, and D. G. Truhlar, Phys. Rev. A **28**, 2740 (1983).
[28]F. Blanco and G. García, Phys. Rev. A **67**, 022701 (2003).
[29]O. Zatsarinny, K. Bartschat, G. Garciá, F. Blanco, L. R. Hargreaves, D. B. Jones, R. Murrie, J. R. Brunton, M. J. Brunger, M. Hoshino, and S. J. Buckman, Phys. Rev. A **83**, 042702 (2011).
[30]I. P. Grant, B. J. McKenzie, P. H. Norrington, D. F. Mayers, and N. C. Pyper, Comput. Phys. Commun. **21**, 207 (1980).
[31]P. Jönsson, G. Gaigalas, J. Bieroń, C. F. Fischer, and I. P. Grant, Comput. Phys. Commun. **184**, 2197 (2013).
[32]Y.-K. Kim and M. E. Rudd, Phys. Rev. A **50**, 3954 (1994).
[33]M. Huttula, S. Heinäsmäki, E. Kukk, R. Sankari, H. Aksela, and S. Aksela, Phys. Rev. A **70**, 022714 (2004).
[34]E. P. F. Lee and A. W. Potts, J. Electron Spectrosc. Relat. Phenom. **19**, 65 (1980).
[35]A. Kramida, Yu. Ralchenko, J. Reader, and NIST ASD Team, *NIST Atomic Spectra Database (ver. 5.7.1)* (National Institute of Standards and Technology, Gaithersburg, MD, 2020), online available at: http://physics.nist.gov/asd; May 10 2020.
[36]M. A. Baig, I. Ahmed, and J. P. Connerade, J. Phys. B: At., Mol. Opt. Phys. **21**, 35 (1988).
[37]M. J. Frisch, G. W. Trucks, H. B. Schlegel, G. E. Scuseria, M. A. Robb *et al.*, Gaussian 09, Revision B.01, Gaussian, Inc., Wallingford, CT, USA, 2010.
[38]C. Lee, W. Yang, and R. G. Parr, Phys. Rev. B **37**, 785 (1988).
[39]C. Sosa, J. Andzelm, B. C. Elkin, E. Wimmer, K. D. Dobbs, and D. A. Dixon, J. Phys. Chem. **96**, 6630 (1992).
[40]C. W. Walter, N. D. Gibson, D. J. Carman, Y.-G. Li, and D. J. Matyas, Phys. Rev. A **82**, 032507 (2010).
[41]C. J. Bostock, D. V. Fursa, and I. Bray, J. Phys. B: At., Mol. Opt. Phys. **45**, 181001 (2012).
[42]K. Bartschat, J. Phys. B: At., Mol. Opt. Phys. **25**, L307 (1992).
[43]L. Ma, J. Indergaard, B. Zhang, I. Larkin, R. Moro, and W. A. de Heer, Phys. Rev. A **91**, 010501(R) (2015).
[44]B. G. Lindsay and M. A. Mangan, in *Photon and Electron Interactions with Atoms, Molecules and Ions*, Landolt-Börnstein Vol. 17C, edited by Y. Itikawa (Springer-Verlag, Berlin, Heidelberg, 2003), Chap. 5.
[45]Y. Itikawa, J. Phys. Chem. Ref. Data **45**, 033106 (2016).
[46]R. P. McEachran, B. P. Marinković, G. García, R. D. White, P. W. Stokes, D. B. Jones, and M. J. Brunger, J. Phys. Chem. Ref. Data **49**, 013102 (2020).
[47]G. J. Boyle, W. J. Tattersall, D. G. Cocks, R. P. McEachran, and R. D. White, Plasma Sources Sci. Technol. **26**, 024007 (2017).
[48]R. D. White, R. E. Robson, B. Schmidt, and M. A. Morrison, J. Phys. D: Appl. Phys. **36**, 3125 (2003).
[49]A. Hochstim, *Kinetic Processes in Gases and Plasmas* (Academic Press, New York, 1969).
[50]L. Campbell and M. J. Brunger, Int. Rev. Phys. Chem. **35**, 297 (2016).
[51]M. J. Brunger, Int. Rev. Phys. Chem. **36**, 333 (2017).
[52]A. I. Lozano, J. C. Oller, D. B. Jones, R. F. da Costa, M. T. do N. Varella, M. H. F. Bettega, F. Ferreira da Silva, P. Limão-Vieira, M. A. P. Lima, R. D. White, M. J. Brunger, F. Blanco, A. Muñoz, and G. García, Phys. Chem. Chem. Phys. **20**, 22368 (2018).
[53]A. I. Lozano, K. Krupa, F. Ferreira da Silva, P. Limão-Vieira, F. Blanco, A. Munõz, D. B. Jones, M. J. Brunger, and G. García, Eur. Phys. J. D **71**, 226 (2017).
[54]F. Costa, A. Traoré-Dubuis, L. Álvarez, A. I. Lozano, X. Ren, A. Dorn, P. Limão-Vieira, F. Blanco, J. C. Oller, A. Muñoz, A. García-Abenza, J. D. Gorfinkiel, A. S. Barbosa, M. H. F. Bettega, P. Stokes, R. D. White, D. B. Jones, M. J. Brunger, and G. García, Int. J. Mol. Sci. **21**, 6947 (2020).